Bio-Inspired Image Restoration

Yuning Cui[1,2], **Wenqi Ren**[1,3]*, **Alois Knoll**[2]
[1]Shenzhen Campus of Sun Yat-sen University
[2]Technical University of Munich
[3]MoE Key Laboratory of Information Technology

Abstract

Image restoration aims to recover sharp, high-quality images from degraded, low-quality inputs. Existing methods have progressively advanced from task-specific designs to general architectures, all-in-one frameworks, and composite degradation handling. Despite these advances, computational efficiency remains a critical factor for practical deployment. In this work, we present BioIR, an efficient and universal image restoration framework inspired by the human visual system. Specifically, we design two bio-inspired modules, Peripheral-to-Foveal (P2F) and Foveal-to-Peripheral (F2P), to emulate the perceptual processes of human vision, with a particular focus on the functional interplay between foveal and peripheral pathways. P2F delivers large-field contextual signals to foveal regions based on pixel-to-region affinity, while F2P propagates fine-grained spatial details through a static-to-dynamic two-stage integration strategy. Leveraging the biologically motivated design, BioIR achieves state-of-the-art performance across three representative image restoration settings: single-degradation, all-in-one, and composite degradation. Moreover, BioIR maintains high computational efficiency and fast inference speed, making it highly suitable for real-world applications. The code and pre-trained models are available at `https://github.com/c-yn/BioIR`.

1 Introduction

Image restoration aims to reconstruct high-quality images from their degraded counterparts [1, 2, 3, 4, 5, 6, 7, 8], which may suffer from quality loss due to adverse weather conditions or the limitations of low-end imaging devices. This task plays a critical role in supporting various downstream perceptual applications [9, 10, 11, 12], such as object detection and depth estimation. In the deep learning era, early methods have primarily focused on addressing *specific* image restoration tasks using Convolutional Neural Networks (CNNs) [13, 14, 15, 16, 17, 18] and Transformer architectures [19, 20, 21, 22, 23, 24]. Subsequently, numerous *general*-purpose methods have been proposed to tackle a variety of tasks using a shared or scalable framework, albeit with separately trained instances for each task [25, 5, 26, 27, 28, 29, 30, 31]. Recently, the concept of *all-in-one* image restoration has emerged, leading to the development of methods that incorporate degradation-aware priors to handle multiple degradations within a single model [32, 33, 34, 35, 36, 37, 38, 39, 40, 41]. The latest advancements have further extended this direction by targeting the *composite degradation* problem, which involves managing multiple degradations simultaneously [42, 43, 44, 35, 45, 46]. A detailed taxonomy of these developments is presented in Figure 1. Despite these advances, most existing algorithms remain tailored to specific scenarios and struggle to generalize effectively across diverse restoration settings.

In addition to generalization capability, computational efficiency is another critical factor for practicability. To this end, extensive efforts have been devoted to improving the efficiency of image restoration models. For instance, numerous studies have sought to enhance the computational efficiency of Transformer-based architectures for high-resolution image restoration by reducing the

*Corresponding author

39th Conference on Neural Information Processing Systems (NeurIPS 2025).

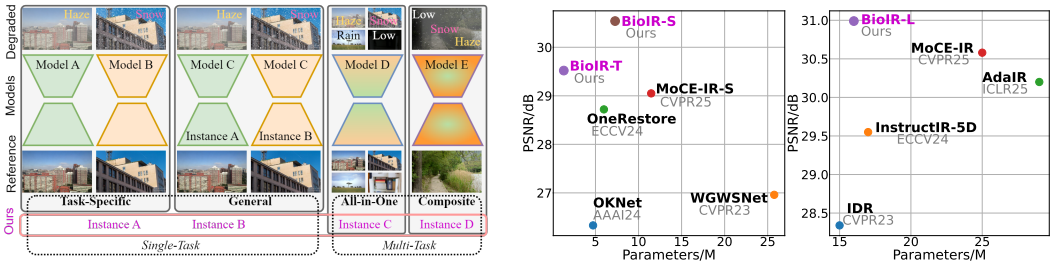

Figure 1: *Left*: Taxonomy of image restoration methods. *Middle*: Comparison of the number of parameters *vs.* PSNR on the CDD11 [42] dataset for composite degradation image restoration. *Right*: Comparison of the number of parameters *vs.* PSNR under the five-task all-in-one setting.

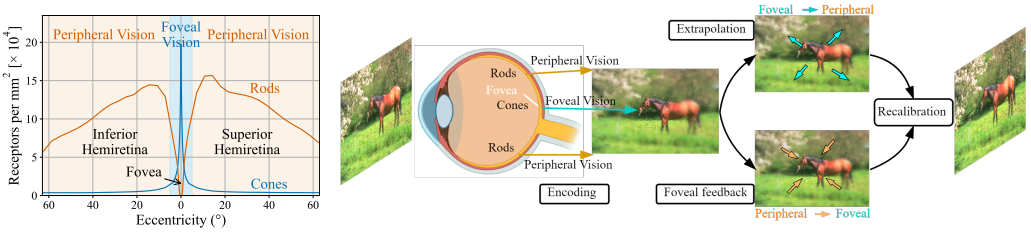

Figure 2: *Left*: Distribution of rod and cone photoreceptors across retinal eccentricity. *Right*: Conceptual overview of foveal–peripheral interactions in human vision. Due to the distinct spatial distributions and functional specializations of rods and cones, peripheral vision supports coarse scene analysis, whereas foveal vision is responsible for detailed processing. The dynamic interplay between these two systems enables the perception of a stable, coherent, and high-fidelity visual experience.

scope of self-attention operations [26, 22, 47, 27, 20, 5]. In contrast, some methods have adopted CNN-based frameworks to achieve high efficiency [30, 48, 49, 50, 51, 31, 6, 52, 53], with a subset of these further incorporating frequency-domain processing to expand the effective receptive field. More recently, a few Mamba-based image restoration algorithms have been proposed, offering an efficient mechanism for capturing long-range dependencies [54, 55, 56, 57, 58, 59, 60, 61, 62, 63, 64, 65].

Taking into account the two critical factors for practical deployment, *universality* and *efficiency*, this paper aims to develop an efficient network for universal image restoration that generalizes well across three representative settings: single-degradation, all-in-one, and composite degradation (see the left part of Figure 1(a)). To this end, we draw inspiration from the remarkable efficiency of the human visual system, whose conceptual overview is illustrated in Figure 2. As shown, the density of cone photoreceptors peaks at the fovea and declines toward the periphery [66], enabling high-acuity detail perception in a limited region. In contrast, peripheral vision covers a much larger portion of the visual field, albeit at lower resolution. After the initial encoding of visual information from both foveal and peripheral pathways, foveal signals are extrapolated to support peripheral representations [67], while peripheral object recognition benefits from integrating large-field contextual information with foveal vision [68]. This interaction is further stabilized through a recalibration process that associates foveal and peripheral inputs into a coherent percept of the visual world.

Inspired by the human perception system, we introduce two bio-inspired modules, termed foveal-to-peripheral (F2P) and peripheral-to-foveal (P2F), to facilitate the interaction between foveal and peripheral visual signals. Specifically, the P2F module delivers large-field contextual signals to local regions by leveraging pixel-to-region affinity. In contrast, the F2P module transmits fine-grained spatial details through a combination of element-wise processing and dynamic integration. The refined foveal and peripheral representations are then recalibrated via element-wise multiplication to enable high-order interactions. Building on these intuitive yet effective designs, we propose BioIR, a bio-inspired image restoration model that achieves state-of-the-art performance across three standardized settings: task-specific, all-in-one, and composite degradation, while maintaining high computational efficiency (see Figure 1). Notably, BioIR can be viewed as a higher-level general-purpose solution that relates to these three categories in much the same way as general architectures

such as Restormer [25] and NAFNet [30] relate to task-specific methods, marking a further step toward universal and practical image restoration. The main contributions are summarized as follows:

- We propose a bio-inspired, efficient, universal image restoration network that leverages two specialized modules to facilitate interaction between foveal and peripheral visual pathways.
- We introduce the foveal-to-peripheral (F2P) module, which transmits fine spatial details through a static-to-dynamic two-stage integration strategy, and the peripheral-to-foveal (P2F) module, which delivers long-range contextual information guided by pixel-to-region affinity.
- Extensive experimental results demonstrate that the proposed model achieves state-of-the-art performance across three representative image restoration settings, including four single-degradation tasks on nine datasets, two all-in-one settings, and two composite degradation benchmarks, while maintaining both high computational efficiency and fast inference speed.

2 Related Work

This section reviews related works from two key perspectives that support the practical application of image restoration methods, namely *versatility* and *efficiency*.

Image Restoration. Early approaches primarily relied on handcrafted priors to constrain the solution space [69, 70, 71]. However, designing effective priors proved to be a non-trivial challenge. Over the past decade, fueled by the rapid progress of deep learning, numerous task-specific methods based on CNNs [13, 72, 73, 18, 16, 52, 74, 75, 76] and Transformer architectures have emerged [21, 19, 22, 20, 77, 24, 78]. These methods learn generalizable priors from large-scale datasets and have demonstrated superior performance over traditional techniques on various image restoration tasks, such as deraining, dehazing, and deblurring. Despite their success, these task-specific methods often struggle to generalize to other restoration tasks due to their specialized design. To address this limitation, general-purpose architectures have gained popularity, offering strong performance across multiple tasks and sometimes even surpassing task-specific methods on their respective targets [79, 80, 29, 48, 31, 49, 30, 26, 81, 27, 82, 6, 28, 83]. For example, Restormer [25] achieves state-of-the-art results on four different tasks through an advanced Transformer architecture. However, these general architectures typically require separately trained instances for each task, forcing users to possess prior knowledge of the degradation type to select the appropriate pre-trained model.

To overcome this challenge, recent research has shifted toward all-in-one solutions that can handle multiple degradation types and levels using a single unified model [84, 41, 38, 85, 86, 87, 88]. These methods are typically trained on compound datasets aggregated from several benchmarks and often incorporate degradation-aware priors extracted from the input images. For instance, PromptIR [34] encodes priors into learnable parameters to guide the restoration process. While these models are well-suited for resource-constrained platforms, they generally assume that each input image is affected by only a single type of degradation. However, real-world scenarios often involve composite degradations, where multiple types of impairments co-occur [89, 90, 35, 91, 92, 93]. For example, night photography commonly suffers from both blurring and low-light conditions due to long exposure in dim environments [43]. Recently, CDD11 [42] was introduced as a comprehensive benchmark comprising 11 categories of degradations, including haze, rain, snow, low light, and their combinations. Correspondingly, composite degradation restoration methods have been developed, such as OneRestore [42] that leverages both textual and visual descriptors to handle these complex scenarios.

Despite these advances, existing methods largely target specific problem categories and struggle to generalize across different restoration settings [18, 25, 34, 94]. In contrast, our model is applicable to three major restoration scenarios, *i.e.,* single-degradation, all-in-one, and composite degradation, by drawing inspiration from the perceptual mechanisms of the human visual system.

Efficient Image Restoration Networks. Efficiency is a critical consideration for practical deployment, enabling faster processing speeds and reduced resource consumption. Recent efforts have focused on improving the computational efficiency of image restoration networks through various strategies. Specifically, several Transformer-based architectures reduce the computational overhead of self-attention by limiting its scope to smaller regions [27, 26, 22, 47, 20], such as windows or strips. In addition, some methods incorporate frequency-domain processing to efficiently model long-range

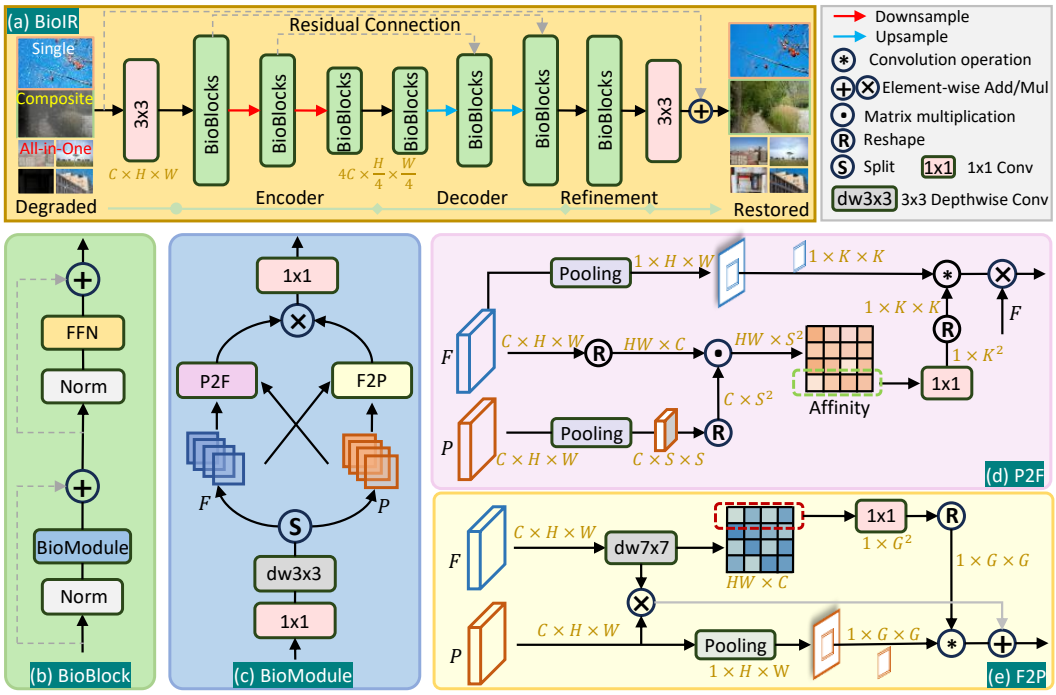

Figure 3: Architectural overview of the proposed BioIR framework for universal image restoration. (a) BioIR adopts a plain U-shaped architecture, with BioBlock (b) serving as the core building block. (c) BioModule enables dynamic interaction between two types of visual signals through the Peripheral-to-Foveal (P2F) and Foveal-to-Peripheral (F2P) modules. (d) P2F delivers large-field contextual information to local regions based on pixel-to-region affinity. (e) F2P propagates fine-grained spatial details by combining element-wise modulation and dynamic convolution.

dependencies [49, 31, 52, 51, 95]. More recently, Mamba-based frameworks have been proposed to achieve global receptive fields through advanced scanning strategies [54, 60, 56, 57, 59, 58, 55, 96].

On another front, significant progress has been made in model compression and acceleration techniques, such as quantization, pruning, and knowledge distillation [97, 98, 99, 100, 101], which further improve inference efficiency without sacrificing performance. Our proposed model is orthogonal to these techniques, providing a strong and efficient baseline that can further benefit from their integration to achieve even greater efficiency and speed.

3 Method

In this section, we first present an overview of the overall pipeline, highlighting the BioBlock as its core component. We then introduce the proposed BioModule, which integrates two key components: the peripheral-to-foveal (P2F) module and the foveal-to-peripheral (F2P) module.

3.1 Overall Pipeline

The schematic of the proposed bio-inspired network for universal image restoration is shown in Figure 3. The network adopts a plain U-shaped architecture to efficiently capture hierarchical features, without relying on advanced designs such as multi-input or multi-output strategies [31]. As illustrated, it consists of three main stages: an encoder, a decoder, and a refinement stage, along with two 3×3 convolutions used to generate feature embeddings and produce the final residual output, respectively.

More specifically, given a degraded image from a single-degradation, all-in-one, or composite degradation setting, the first 3×3 convolution embeds the 3-channel input into a feature map of size $C \times H \times W$. The encoder then progressively reduces the spatial resolution while expanding the channel dimension, resulting in a deep feature map of size $4C \times \frac{H}{4} \times \frac{W}{4}$. The decoder subsequently

restores the feature resolution back to $C \times H \times W$, with feature-level residual connections to assist the restoration process. The refinement stage further enhances the decoded feature maps [25, 29, 34]. Finally, the second 3×3 convolution produces a residual image, which is added to the degraded input via an image-level residual connection to obtain the final restored image.

The three stages are primarily composed of different numbers of BioBlocks, with architectural details illustrated in Figure 3(b). Each BioBlock follows a Transformer-style design but replaces the self-attention mechanism with the proposed BioModule, as shown in Figure 3(c). Given input features X, the computation within a BioBlock can be formulated as follows:

$$\hat{X} = \mathcal{F}(\mathcal{N}(\tilde{X})) + \tilde{X}, \quad \text{where} \quad \tilde{X} = \mathcal{B}(\mathcal{N}(X)) + X, \tag{1}$$

where $\hat{X}$ is the output of the BioBlock. Here, $\mathcal{N}$ denotes the normalization layer, while $\mathcal{B}$ and $\mathcal{F}$ represent the BioModule and the feed-forward network (FFN) [25], respectively.

3.2 Bio-Inspired Module (BioModule)

Inspired by the human visual system, which processes different types of visual signals through distinct pathways and integrates them to form a coherent perception, the proposed BioModule adopts a two-branch design that mimics this biological mechanism. Specifically, the input feature map $X \in \mathbb{R}^{C \times H \times W}$ is first refined using a 1×1 convolution followed by a 3×3 depth-wise convolution. Next, two specialized modules, P2F and F2P, are employed to extract complementary feature representations and facilitate their interaction. These features are then recalibrated via element-wise multiplication to integrate the two information streams. Finally, a 1×1 convolution produces the output feature map. The overall computation of the BioModule can be formally expressed as:

$$\hat{X} = \text{Conv}_{1\times1}(\text{P2F}(F, P) \otimes \text{F2P}(P, F)), \tag{2}$$

$$P, F = \text{Split}(\text{DWConv}_{3\times3}(\text{Conv}_{1\times1}(X))), \tag{3}$$

where *DWConv* and *Conv* denote depth-wise convolution and standard convolution, respectively, with the subscript indicating the kernel size. The *Split* operation evenly divides the feature map along the channel dimension into two parts, denoted as P and F. Notably, the 1×1 convolution in Eq. (3) doubles the channel dimension to facilitate this splitting operation.

3.2.1 Peripheral-to-Foveal Module (P2F)

The P2F module delivers large-field visual signals to local spatial regions by equipping convolution operations with knowledge of long-range dependencies. To achieve this, it encodes the contextual relationships between each pixel and its surrounding regions by computing the affinity between the pixel and a set of region-representative pixels. These affinity values are then integrated through convolutional operations to dynamically generate pixel-specific convolution kernels. This enables the injection of global contextual signals into local regions via sliding-window convolutions, effectively enhancing local representations with long-range information.

The architectural details of P2F are illustrated in Figure 3(d). Given the input feature map $P \in \mathbb{R}^{C \times H \times W}$, average pooling is first applied to extract contextual representations of size $C \times S \times S$, which are then reshaped to $C \times S^2$ for affinity computation. Specifically, the affinity map A is computed between these contextual features and the reshaped feature map P:

$$A = \mathcal{R}(F) \odot \mathcal{R}(\text{Pool}(P)) \in \mathbb{R}^{HW \times S^2}, \tag{4}$$

where $\mathcal{R}$ and *Pool* denote the reshaping and average pooling operations, respectively, and $\odot$ represents matrix multiplication. Each element in the affinity map A encodes the relationship between a pixel and a specific region. Next, a 1×1 convolution is applied row-wise to A to generate pixel-specific convolution kernels of size $1 \times K^2$, effectively injecting contextual information into every weight of these kernels by establishing pixel-to-region interactions.

To apply the learned kernels to F, we first perform average pooling on F to obtain channel-compressed features of size $1 \times H \times W$, improving computational efficiency. These compressed features are then convolved with the learned kernels to produce enhanced features of size $1 \times H \times W$, which are used as attention scores to modulate F, resulting in the final output of the P2F module.

3.2.2 Foveal-to-Peripheral Module (F2P)

In contrast to P2F, which focuses on delivering global contextual information, the proposed F2P module aims to propagate fine-grained spatial details. As illustrated in Figure 3(e), F2P employs a static-to-dynamic integration strategy, element-wise modulation followed by dynamic convolution, to fully leverage the detailed local information. Specifically, given input $F \in \mathbb{R}^{C\times H\times W}$, a depth-wise convolution is first applied to extract locally refined representations. These refined features are then used to directly modulate the features P through element-wise multiplication, formally expressed as:

$$\hat{X}_1 = P \otimes \tilde{F}, \quad \text{where } \tilde{F} = \text{DWConv}_{7\times 7}(F). \tag{5}$$

In addition, $\tilde{F}$ is further utilized to generate convolutional kernels for refining P in a dynamic, pixel-wise manner. Specifically, $\tilde{F}$ is passed through a 1×1 convolution to produce pixel-specific kernels. In parallel, the features P are compressed to a spatial map of size $1 \times H \times W$ to enhance computational efficiency. These compressed features are then convolved with the learned kernels to integrate fine-grained information. Finally, the outputs from the element-wise modulation and the convolutional refinement stages are combined via addition, which can be formally expressed as:

$$\hat{X} = \hat{X}_1 + \hat{X}_2, \quad \text{where} \quad \hat{X}_2 = \text{Pool}(P) \circledast \text{Conv}_{1\times 1}(\tilde{F}), \tag{6}$$

where $\circledast$ denotes the convolution operation.

4 Experiments and Analysis

To validate the effectiveness of the proposed model, we conduct extensive experiments across three image restoration settings: **(a)** single-degradation, **(b)** all-in-one, and **(c)** composite degradation.

- Single-degradation: The model is separately trained on nine datasets covering four restoration tasks, including image desnowing, dehazing, deraining, and low-light image enhancement.
- All-in-one: The model is evaluated under two sub-settings: three-task and five-task. It is trained on a compound dataset comprising three or five different tasks and tested on the corresponding test sets, where each image is affected by a single type of degradation.
- Composite degradation: The model is assessed on two benchmarks, LOLBlur [43] and CDD11 [42], where images suffer from up to two or three simultaneous degradation types.

We scale the model according to the complexity of the datasets to ensure a balanced trade-off between performance and efficiency. Further details on training configurations and additional results are provided in the supplementary material. In the following tables, the best and second-best results are highlighted in magenta and blue, respectively. FLOPs are calculated on a $3 \times 256 \times 256$ input patch.

4.1 Single-Degradation Image Restoration

Image desnowing. We evaluate the proposed model on three widely used datasets for image desnowing: Snow100K [15], SRRS [102], and CSD [74]. As shown in Table 1(a), our model significantly outperforms the recent Transformer-based architecture MBTF-L V2 [29] on both Snow100K and SRRS, while requiring lower computational complexity.

Image dehazing. We compare our tiny model with lightweight state-of-the-art algorithms on the SOTS-Indoor [103] dataset for image dehazing. As reported in Table 1(b), the proposed BioIR-T achieves a notable performance improvement of 1.05 dB in PSNR over the recent Mamba-based MaIR [59], while using only 39% of its parameters. In addition, we evaluate our base model against heavyweight dehazing methods on the Haze4K [104] dataset. Table 1(c) further demonstrates the superior performance of our model in this more challenging setting.

Low-light image enhancement. We further evaluate the proposed model on the LOLv2-s [105] dataset for low-light image enhancement. The quantitative results, summarized in Table 1(d), show that our tiny model outperforms the recent Mamba-based enhancer [60] by 0.36 dB in PSNR, while using fewer parameters and achieving lower computational complexity.

Image deraining. We first evaluate our model on the raindrop removal dataset AGAN-Data [106]. Table 1(e) shows that our model achieves a notable PSNR improvement of 0.66 dB over the recent

Table 1: Quantitative results on nine datasets across four single-degradation image restoration tasks.

(a) Snow100K, SRRS, and CSD for desnowing

Method	Snow100K PSNR	Snow100K SSIM	SRRS PSNR	SRRS SSIM	CSD PSNR	CSD SSIM	Params (M)	FLOPs (G)
FocalNet$_{ICCV23}$ [28]	33.53	0.95	31.34	0.98	37.18	0.99	3.74	30.6
IRNeXt$_{ICML23}$ [48]	33.61	0.95	31.91	0.98	37.29	0.99	5.46	42.1
MBTF-L V1$_{ICCV23}$ [24]	33.79	0.95	32.26	0.98	-	-	7.43	88.1
ConvIR-B$_{PAMI24}$ [31]	33.92	0.96	32.39	0.98	39.10	0.99	8.63	71.2
MBTF-L V2$_{PAMI25}$ [29]	34.01	0.96	32.55	0.98	-	-	7.29	86.0
BioIR-B$_{Ours}$	34.44	0.96	32.67	0.98	39.19	0.99	7.28	67.81

(b) SOTS-Indoor for dehazing

Method	PSNR	SSIM	Params	FLOPs
DeHamer$_{CVPR22}$ [19]	36.63	0.988	132.45	48.93
Fourmer$_{ICML23}$ [49]	37.32	0.990	1.29	20.6
DehazeFormer$_{TIP23}$ [20]	38.46	0.994	4.63	48.64
OKNet-S$_{AAAI24}$ [3]	37.59	0.994	2.40	17.86
DEA-Net$_{TIP24}$ [111]	39.16	0.992	2.84	24.88
MaIR$_{CVPR25}$ [59]	39.45	0.997	3.40	24.03
BioIR-T$_{Ours}$	40.50	0.997	1.32	16.65

(c) Haze4K for dehazing

Method	PSNR	SSIM	Params	FLOPs
PMNet$_{ECCV22}$ [112]	33.49	0.98	18.90	81.1
FSNet$_{PAMI23}$ [79]	34.12	0.99	13.29	110.5
ConvIR-B$_{PAMI24}$ [31]	34.15	0.99	8.63	71.2
ConvIR-L$_{PAMI24}$ [31]	34.50	0.99	14.83	129.9
MBTF V1$_{ICCV23}$ [24]	34.47	0.99	7.43	88.1
MBTF V2$_{PAMI25}$ [29]	34.92	0.99	7.29	86.0
BioIR-B$_{Ours}$	35.62	0.99	7.28	67.81

(d) LOLv2-s for low-light enhancement

Method	PSNR	SSIM	Params	FLOPs
MIRNet$_{ECCV20}$ [113]	21.94	0.876	31.76	785
Restormer$_{CVPR22}$ [25]	21.41	0.830	26.13	144.25
SNR-Net$_{CVPR22}$ [114]	24.14	0.928	4.01	26.35
Retinexformer$_{ICCV23}$ [23]	25.67	0.930	1.61	15.57
MambaIR$_{ECCV24}$ [54]	25.55	0.929	4.30	60.66
MambaLLIE$_{NeurIPS24}$ [60]	25.87	0.940	2.28	20.85
BioIR-T$_{Ours}$	26.22	0.947	1.32	16.65

(e) AGAN for raindrop

Method	PSNR	SSIM
Restormer$_{CVPR22}$ [25]	31.68	0.934
IDT$_{PAMI22}$ [115]	31.87	0.931
MAXIM$_{CVPR22}$ [116]	31.87	0.935
AWRCP$_{ICCV23}$ [117]	31.93	0.931
FPro$_{ECCV24}$ [118]	31.96	0.937
AST$_{CVPR24}$ [107]	32.32	0.935
BioIR-T$_{Ours}$	32.98	0.944

(f) DID-Data and SPA-Data for rain streak removal

Method	DID-Data PSNR	DID-Data SSIM	SPA-Data PSNR	SPA-Data SSIM	Params (M)	FLOPs (G)
Uformer$_{CVPR22}$ [27]	35.02	0.9621	46.13	0.9913	50.88	45.9
Restormer$_{CVPR22}$ [25]	35.29	0.9641	47.98	0.9921	26.13	144.25
IDT$_{PAMI22}$ [115]	34.89	0.9623	47.35	0.9930	16.41	61.9
DRSformer$_{CVPR23}$ [21]	35.35	0.9646	48.54	0.9924	33.65	242.9
NeRD-Rain-S$_{CVPR24}$ [110]	35.36	0.9647	48.90	0.9936	10.53	79.2
BioIR-B$_{Ours}$	35.62	0.9668	49.39	0.9933	7.28	67.81

Table 2: Runtime on NVIDIA RTX 4090 GPU

(a) Single-degradation task

Task/Data	Method	Time/s	PSNR
Desnowing	MBTF-L V2	0.558	34.01
Snow100K	**Ours**	0.133	34.44
Deraining	AST	0.389	32.32
AGAN	**Ours**	0.083	32.98
Enhance	MambaLLIE	0.093	25.87
LOLv2-s	**Ours**	0.038	26.22

(b) All-in-one task

Method	Time/s	PSNR 5D	PSNR 3D
PromptIR	0.147	29.15	32.06
AdaIR	0.144	30.20	32.69
MoCE-IR	0.112	30.58	32.73
Ours	0.132	30.99	32.87

Table 3: Quantitative results under the three-task all-in-one setting. σ indicates the noise level.

Method	Params	*Dehazing* SOTS PSNR	*Dehazing* SOTS SSIM	*Deraining* Rain100L PSNR	*Deraining* Rain100L SSIM	*Denoising* BSD68$_{\sigma=15}$ PSNR	BSD68$_{\sigma=15}$ SSIM	BSD68$_{\sigma=25}$ PSNR	BSD68$_{\sigma=25}$ SSIM	BSD68$_{\sigma=50}$ PSNR	BSD68$_{\sigma=50}$ SSIM	Average PSNR	Average SSIM
PromptIR$_{NeurIPS23}$ [34]	36M	30.58	0.974	36.37	0.972	33.98	0.933	31.31	0.888	28.06	0.799	32.06	0.913
Art-PromptIR$_{MM24}$ [119]	33M	30.83	0.979	37.94	0.982	34.06	0.934	31.42	0.891	28.14	0.801	32.49	0.917
UniProcessor$_{ECCV24}$ [120]	1002M	31.66	0.979	38.17	0.982	34.08	0.935	31.42	0.891	28.17	0.803	32.70	0.918
AdaIR$_{ICLR25}$ [37]	29M	31.06	0.980	38.64	0.983	34.12	0.935	31.45	0.892	28.19	0.802	32.69	0.918
MoCE-IR$_{CVPR25}$ [35]	25M	31.34	0.979	38.57	0.984	34.11	0.932	31.45	0.888	28.18	0.800	32.73	0.917
BioIR-L$_{Ours}$	16M	31.69	0.981	38.63	0.984	34.19	0.937	31.54	0.895	28.28	0.809	32.87	0.921

AST [107] algorithm. In addition, we conduct experiments on two benchmark datasets, DID-Data [108] and SPA-Data [109], for rain streak removal. The results, reported in Table 1(f), demonstrate that our model outperforms the specialized method NeRD-Rain-S [110], achieving a PSNR gain of 0.49 dB on the real-world SPA-Data [109] while maintaining lower computational cost.

Inference speed comparison. Table 2(a) presents runtime comparisons with leading algorithms on three single-degradation tasks. As shown, the proposed model achieves superior performance while maintaining faster inference speed, highlighting its practical efficiency.

4.2 All-in-One Image Restoration

Three-task setting. We begin by evaluating our model under the three-task all-in-one image restoration setting. The model is trained on a compound dataset combining three tasks: dehazing, deraining, and denoising. It is then tested on the corresponding test sets for these tasks. As shown in Table 3, our model achieves the best performance across nearly all evaluation metrics, with an average PSNR improvement of 0.14 dB over the second-best method [35]. Notably, on the BSD68 [123] dataset for image denoising, our model achieves substantial performance improvements across three different noise levels, while requiring fewer parameters than competing methods.

Five-task setting. Following prior works [36, 35, 37], we further evaluate our model under the five-task all-in-one setting. In addition to the three previously considered tasks, we include the GoPro [124] and LOLv1 [125] datasets for motion deblurring and low-light enhancement, respectively. As shown

19.98 dB	18.40 dB	19.02 dB	24.74 dB	30.29 dB	PSNR/+∞
Rainy Image	InstructIR-5D [36]	AdaIR [37]	MoCE-IR [35]	BioIR-L	Reference

Figure 4: Visual results on the Rain100L [121] dataset under the five-task all-in-one setting.

Table 4: Quantitative comparisons under the five-task setting for all-in-one image restoration.

Method	Params	*Dehazing* SOTS PSNR	SOTS SSIM	*Deraining* Rain100L PSNR	Rain100L SSIM	*Denoising* BSD68$_{\sigma=25}$ PSNR	BSD68$_{\sigma=25}$ SSIM	*Deblurring* GoPro PSNR	GoPro SSIM	*Low-Light* LOLv1 PSNR	LOLv1 SSIM	Average PSNR	Average SSIM
IDR$_{\text{CVPR23}}$ [33]	15M	25.24	0.943	35.63	0.965	31.60	0.887	27.87	0.846	21.34	0.826	28.34	0.893
PromptIR$_{\text{NeurIPS23}}$ [34]	36M	26.54	0.949	36.37	0.970	31.47	0.886	28.71	0.881	22.68	0.832	29.15	0.904
Gridformer$_{\text{IJCV24}}$ [122]	34M	26.79	0.951	36.61	0.971	31.45	0.885	29.22	0.884	22.59	0.831	29.33	0.904
InstructIR-5D$_{\text{ECCV24}}$ [36]	17M	27.10	0.956	36.84	0.973	31.40	0.873	29.40	0.886	23.00	0.836	29.55	0.908
AdaIR$_{\text{ICLR25}}$ [37]	29M	30.53	0.978	38.02	0.981	31.35	0.889	28.12	0.858	23.00	0.845	30.20	0.910
MoCE-IR$_{\text{CVPR25}}$ [35]	25M	30.48	0.974	38.04	0.982	31.34	0.887	30.05	0.899	23.00	0.852	30.58	0.919
BioIR-L$_{\text{Ours}}$	16M	31.77	0.981	38.75	0.985	31.52	0.894	29.61	0.889	23.29	0.862	30.99	0.922

Table 5: PSNR results of directly applying the model pre-trained under the five-task all-in-one setting to three denoising datasets: BSD68 [123], Urban100 [127], and Kodak24 [128].

Method	BSD68 [123] $\sigma=15$	BSD68 $\sigma=25$	BSD68 $\sigma=50$	Urban100 [127] $\sigma=15$	Urban100 $\sigma=25$	Urban100 $\sigma=50$	Kodak24 [128] $\sigma=15$	Kodak24 $\sigma=25$	Kodak24 $\sigma=50$	Average
TransWeather$_{\text{CVPR22}}$ [129]	31.16	29.00	26.08	29.64	27.97	26.08	31.67	29.64	26.74	28.66
IDR$_{\text{CVPR23}}$ [33]	34.11	31.60	28.14	33.82	31.29	28.07	34.78	32.42	29.13	31.48
InstructIR-5D$_{\text{ECCV24}}$ [36]	34.00	31.40	28.15	33.77	31.40	28.13	34.70	32.26	29.16	31.44
MoCE-IR$_{\text{CVPR25}}$ [35]	34.00	31.34	28.07	34.01	31.59	28.20	34.87	32.38	29.20	31.52
AdaIR$_{\text{ICLR25}}$ [37]	34.01	31.35	28.06	34.10	31.68	28.29	34.89	32.38	29.21	31.55
BioIR-L$_{\text{Ours}}$	34.18	31.52	28.27	34.50	32.16	28.92	35.15	32.67	29.55	31.88

in Table 4, our model achieves the best results in most categories. Notably, it establishes a new state-of-the-art by outperforming the second-best algorithm, MoCE-IR [35], with an average PSNR improvement of 0.41 dB across all datasets. While MoCE-IR achieves higher scores on the GoPro dataset, this is primarily due to its reliance on a specialized motion deblurring backbone [126]. Additionally, our model surpasses the recent frequency-based AdaIR [37] by a notable margin of 0.79 dB in PSNR. Importantly, these improvements are achieved with fewer parameters, highlighting the efficiency and effectiveness of our bio-inspired design. Visual results in Figure 4 further demonstrate the superiority of our model, showing that its output is significantly closer to the reference image, whereas the first two methods produce results that perform even worse than the degraded rainy input.

Additionally, we assess the generalization capability of our model by directly applying it to unseen denoising datasets, including Urban100 [127] and Kodak24 [128]. As reported in Table 5, our model consistently outperforms recent strong competitors across all evaluation metrics. In particular, it achieves a notable average PSNR improvement of 0.34 dB over the heavyweight AdaIR [37], further demonstrating its robustness and generalization ability.

Runtime comparison. Table 2(b) reports the inference time of state-of-the-art all-in-one algorithms on the Rain100L [121] dataset. As shown, our model achieves significantly higher accuracy than the competing methods under both settings, while maintaining a comparable inference speed.

Discussion. Despite not relying on any explicit degradation-related priors, as employed in previous methods [34, 32, 37], our model achieves strong performance in both all-in-one settings. We attribute this success to two key factors: (*i*) the large-field signals extracted by the peripheral vision branch, which capture the contextual information of degraded images and can serve as implicit priors to guide the restoration of local details in each module; and (*ii*) the bio-inspired architecture, which endows the model with powerful representation learning capabilities, enabling it to recover sharp features from degraded inputs without relying on explicit, task-specific priors.

Table 6: Quantitative evaluation on the LOLBlur [43] dataset for composite degradation.

Method Venue	MIMO [1] ICCV21	NAFNet [30] ECCV22	LEDNet [43] ECCV22	Restormer [25] CVPR22	RetinexFormer [23] ICCV23	DarkIR-M [44] CVPR25	DarkIR-L [44] CVPR25	**BioIR-T** Ours
PSNR	22.41	25.36	25.74	26.72	26.02	27.00	27.30	27.70
SSIM	0.835	0.882	0.850	0.902	0.887	0.883	0.898	0.908
Params (M)	6.8	12.05	7.4	26.13	1.61	3.31	12.96	1.32

Table 7: Quantitative comparison for composite degradation image restoration on the 11 degradation categories of the CDD11 [42] dataset. Results are reported in terms of PSNR and SSIM.

Method	Params	Low (L)		Haze (H)		Rain (R)		Snow (S)		L+H		L+R		L+S		H+R		H+S		L+H+R		L+H+S		Average	
AirNet	9M	24.83	.778	24.21	.951	26.55	.891	26.79	.919	23.23	.779	22.82	.710	23.29	.723	22.21	.868	23.29	.901	21.80	.708	22.24	.725	23.75	.814
PromptIR	36M	26.32	.805	26.10	.969	31.56	.946	31.53	.960	24.49	.789	25.05	.771	24.51	.761	24.54	.924	23.70	.925	23.74	.752	23.33	.747	25.90	.850
WGWSNet	26M	24.39	.774	27.90	.982	33.15	.964	34.43	.973	24.27	.800	25.06	.772	24.60	.765	27.23	.955	27.65	.960	23.90	.772	23.97	.771	26.96	.863
WeatherDiff	83M	23.58	.763	21.99	.904	24.85	.885	24.80	.888	21.83	.756	22.69	.730	22.12	.707	21.25	.868	21.99	.868	21.23	.716	21.04	.698	22.49	.799
OneRestore	6M	26.48	.826	32.52	.990	33.40	.964	34.31	.973	25.79	.822	25.58	.799	25.19	.789	29.99	.957	30.21	.964	24.78	.788	24.90	.791	28.47	.878
MoCE-IR-S	11M	27.26	.824	32.66	.990	34.31	.970	35.91	.980	26.24	.817	26.25	.800	26.04	.793	29.93	.964	30.19	.970	25.41	.789	25.39	.790	29.05	.881
BioIR-T	1M	27.14	.834	34.77	.992	34.48	.970	36.26	.979	26.11	.830	26.17	.809	26.01	.804	31.64	.968	31.60	.972	25.22	.799	25.34	.802	29.52	.887
BioIR-B	7M	27.52	.838	36.95	.995	35.35	.974	37.28	.981	26.79	.835	26.78	.817	26.63	.812	32.77	.973	33.39	.977	26.20	.811	26.28	.811	30.54	.893

Table 8: Ablation results for the proposed bio-inspired components and alternative design choices.

(a) Ablation studies for individual components.

Recalibration	P2F	F2P	PSNR	FLOPs	Params
			33.18	15.15	1.31
✓			33.67	14.34	1.23
	✓		36.64	15.38	1.25
		✓	36.96	15.61	1.29
✓	✓	✓	38.26	16.65	1.32

(b) Peripheral vision scope (S^2, Fig. 3d).

Scope	PSNR	FLOPs	Params
1×1	36.10	14.37	1.23
2×2	36.27	14.38	1.23
4×4	36.20	14.43	1.23
8×8	36.45	14.62	1.23
16×16	36.64	15.38	1.25

(c) Foveal vision scope (dw, Fig. 3e).

Kernel	PSNR	FLOPs	Params
1×1	34.49	14.53	1.24
3×3	35.32	14.66	1.24
5×5	36.10	14.93	1.26
7×7	36.59	15.33	1.28
9×9	36.83	15.87	1.30

4.3 Composite Degradation Image Restoration

Two-degradation setting. We first evaluate our model on the LOLBlur [43] dataset, which presents a composite degradation scenario involving both low-light conditions and blur. Table 6 shows that our model significantly outperforms the recent specialized method DarkIR-L [44] by 0.4 dB, while requiring only 10% of its parameters. Compared to DarkIR-M, our model achieves an even larger improvement of up to 0.7 dB in PSNR, while using less than half the number of parameters.

Three-degradation setting. We further compare our model against state-of-the-art multi-task image restoration methods on the more challenging CDD11 [42] dataset, which involves composite degradations across 11 degradation categories, with each image affected by up to three simultaneous degradation types. As reported in Table 7, our base model, BioIR-B, consistently achieves the best performance across all evaluation metrics, significantly outperforming the second-best method, MoCE-IR-S, by an average margin of 1.02 dB in PSNR. Notably, our tiny model, BioIR-T, surpasses most competing methods on the majority of metrics while using only approximately 1M parameters, highlighting the efficiency of our design.

4.4 Ablation Study

We conduct ablation studies by training the dehazing model on the RESIDE-Indoor [103] dataset for 100k iterations and evaluating its performance on the corresponding SOTS-Indoor [103] test set. More ablation study results are provided in the supplementary material.

Effects of individual components. Table 8(a) presents the results of adding the proposed components to a baseline model, which consists of only two 1×1 convolutions and a 3×3 depth-wise convolution within the BioModule. This baseline achieves 33.18 dB on the SOTS-Indoor [103] dataset. Introducing feature splitting and the recalibration mechanism via element-wise multiplication improves the performance by 0.49 dB, while slightly reducing computational overhead. Adding the two key components, P2F and F2P, boosts performance by 3.46 dB and 3.78 dB over the baseline, respectively, demonstrating the effectiveness of the proposed bio-inspired design. Finally, applying recalibration to the outputs of both P2F and F2P yields the best result, achieving a 5.08 dB PSNR improvement over the baseline with only a negligible increase in computational cost.

Peripheral vision scope. The peripheral vision branch in P2F provides large-field contextual signals to support foveal processing. We investigate the effect of varying the peripheral vision scope, which is controlled by the spatial resolution S^2 of the pooled feature map (Figure 3d). A larger S corresponds to a smaller peripheral field. As shown in Table 8(b), increasing S generally improves performance, suggesting that a more focused peripheral scope benefits the model. In our final design, we adopt a resolution of 16×16, which provides a favorable trade-off between performance and efficiency.

Foveal vision scope. The foveal vision branch in F2P delivers fine-grained spatial information to the peripheral pathway. As shown in Table 8(c), expanding the spatial extent of foveal processing consistently improves performance, but at the expense of increased computational cost. This observation aligns with the biological organization of the human visual system, where the separation and cooperation of foveal and peripheral pathways are essential for achieving both stability and efficiency in perception. Based on this trade-off, we adopt a kernel size of 7×7 in our final model to achieve a balanced compromise between accuracy and computational efficiency.

5 Conclusion

This study presents an efficient and universal image restoration network inspired by the human visual system. Specifically, the proposed peripheral-to-foveal (P2F) module extracts large-field contextual signals and integrates them into local regions to guide the restoration process, while the foveal-to-peripheral (F2P) module propagates fine-grained local features to enhance peripheral representations. A recalibration mechanism further harmonizes these two complementary information streams. Built upon this simple yet highly effective bio-inspired design, the proposed BioIR network achieves state-of-the-art performance across three major categories of image restoration tasks, including nine datasets for four single-degradation tasks, two all-in-one task settings, and two composite degradation benchmarks, while maintaining high computational efficiency and fast inference speed.

Acknowledgement

This work was supported by the National Natural Science Foundation of China under Grants 62311530686, 62322216, U24B20175, the Guangdong Basic and Applied Basic Research Foundation under Grant 2023A1515012839, and the Fundamental Research Funds for the Central Universities, Sun Yat-sen University under Grant 23lgbj015.

References

[1] Sung-Jin Cho, Seo-Won Ji, Jun-Pyo Hong, Seung-Won Jung, and Sung-Jea Ko. Rethinking coarse-to-fine approach in single image deblurring. In *ICCV*, 2021.

[2] Haoyu Chen, Wenbo Li, Jinjin Gu, Jingjing Ren, Sixiang Chen, Tian Ye, Renjing Pei, Kaiwen Zhou, Fenglong Song, and Lei Zhu. Restoreagent: Autonomous image restoration agent via multimodal large language models. In *NeurIPS*, 2024.

[3] Yuning Cui, Wenqi Ren, and Alois Knoll. Omni-kernel network for image restoration. In *AAAI*, 2024.

[4] Cong Wang, Jinshan Pan, Wei Wang, Jiangxin Dong, Mengzhu Wang, Yakun Ju, and Junyang Chen. Promptrestorer: A prompting image restoration method with degradation perception. In *NeurIPS*, 2023.

[5] Xiangyu Chen, Zheyuan Li, Yuandong Pu, Yihao Liu, Jiantao Zhou, Yu Qiao, and Chao Dong. A comparative study of image restoration networks for general backbone network design. In *ECCV*, 2024.

[6] Xingyu Jiang, Xiuhui Zhang, Ning Gao, and Yue Deng. When fast fourier transform meets transformer for image restoration. In *ECCV*, 2024.

[7] Junjun Jiang, Zengyuan Zuo, Gang Wu, Kui Jiang, and Xianming Liu. A survey on all-in-one image restoration: Taxonomy, evaluation and future trends. *arXiv preprint arXiv:2410.15067*, 2024.

[8] Yuning Cui and Alois Knoll. Dual-domain strip attention for image restoration. *NN*, 2024.

[9] Shangquan Sun, Wenqi Ren, Tao Wang, and Xiaochun Cao. Rethinking image restoration for object detection. *NeurIPS*, 2022.

[10] Xin Yang, Wending Yan, Yuan Yuan, Michael Bi Mi, and Robby T Tan. Semantic segmentation in multiple adverse weather conditions with domain knowledge retention. In *AAAI*, 2024.

[11] Haimei Zhao, Jing Zhang, Zhuo Chen, Shanshan Zhao, and Dacheng Tao. Unimix: Towards domain adaptive and generalizable lidar semantic segmentation in adverse weather. In *CVPR*, 2024.

[12] Kieran Saunders, George Vogiatzis, and Luis J Manso. Self-supervised monocular depth estimation: Let's talk about the weather. In *ICCV*, 2023.

[13] Bolun Cai, Xiangmin Xu, Kui Jia, Chunmei Qing, and Dacheng Tao. Dehazenet: An end-to-end system for single image haze removal. *IEEE TIP*, 2016.

[14] Xueyang Fu, Jiabin Huang, Delu Zeng, Yue Huang, Xinghao Ding, and John Paisley. Removing rain from single images via a deep detail network. In *CVPR*, 2017.

[15] Yun-Fu Liu, Da-Wei Jaw, Shih-Chia Huang, and Jenq-Neng Hwang. Desnownet: Context-aware deep network for snow removal. *IEEE TIP*, 2018.

[16] Lingyan Ruan, Bin Chen, Jizhou Li, and Miuling Lam. Learning to deblur using light field generated and real defocus images. In *CVPR*, 2022.

[17] Xiaohong Liu, Yongrui Ma, Zhihao Shi, and Jun Chen. Griddehazenet: Attention-based multi-scale network for image dehazing. In *ICCV*, 2019.

[18] Xu Qin, Zhilin Wang, Yuanchao Bai, Xiaodong Xie, and Huizhu Jia. Ffa-net: Feature fusion attention network for single image dehazing. In *AAAI*, 2020.

[19] Chun-Le Guo, Qixin Yan, Saeed Anwar, Runmin Cong, Wenqi Ren, and Chongyi Li. Image dehazing transformer with transmission-aware 3d position embedding. In *CVPR*, 2022.

[20] Yuda Song, Zhuqing He, Hui Qian, and Xin Du. Vision transformers for single image dehazing. *IEEE TIP*, 2023.

[21] Xiang Chen, Hao Li, Mingqiang Li, and Jinshan Pan. Learning a sparse transformer network for effective image deraining. In *CVPR*, 2023.

[22] Fu-Jen Tsai, Yan-Tsung Peng, Yen-Yu Lin, Chung-Chi Tsai, and Chia-Wen Lin. Stripformer: Strip transformer for fast image deblurring. In *ECCV*, 2022.

[23] Yuanhao Cai, Hao Bian, Jing Lin, Haoqian Wang, Radu Timofte, and Yulun Zhang. Retinexformer: One-stage retinex-based transformer for low-light image enhancement. In *ICCV*, 2023.

[24] Yuwei Qiu, Kaihao Zhang, Chenxi Wang, Wenhan Luo, Hongdong Li, and Zhi Jin. Mb-taylorformer: Multi-branch efficient transformer expanded by taylor formula for image dehazing. In *ICCV*, 2023.

[25] Syed Waqas Zamir, Aditya Arora, Salman Khan, Munawar Hayat, Fahad Shahbaz Khan, and Ming-Hsuan Yang. Restormer: Efficient transformer for high-resolution image restoration. In *CVPR*, 2022.

[26] Jingyun Liang, Jiezhang Cao, Guolei Sun, Kai Zhang, Luc Van Gool, and Radu Timofte. Swinir: Image restoration using swin transformer. In *ICCVW*, 2021.

[27] Zhendong Wang, Xiaodong Cun, Jianmin Bao, Wengang Zhou, Jianzhuang Liu, and Houqiang Li. Uformer: A general u-shaped transformer for image restoration. In *CVPR*, 2022.

[28] Yuning Cui, Wenqi Ren, Xiaochun Cao, and Alois Knoll. Focal network for image restoration. In *ICCV*, 2023.

[29] Zhi Jin, Yuwei Qiu, Kaihao Zhang, Hongdong Li, and Wenhan Luo. Mb-taylorformer v2: Improved multi-branch linear transformer expanded by taylor formula for image restoration. *IEEE TPAMI*, 2025.

[30] Liangyu Chen, Xiaojie Chu, Xiangyu Zhang, and Jian Sun. Simple baselines for image restoration. In *ECCV*, 2022.

[31] Yuning Cui, Wenqi Ren, Xiaochun Cao, and Alois Knoll. Revitalizing convolutional network for image restoration. *IEEE TPAMI*, 2024.

[32] Boyun Li, Xiao Liu, Peng Hu, Zhongqin Wu, Jiancheng Lv, and Xi Peng. All-in-one image restoration for unknown corruption. In *CVPR*, 2022.

[33] Jinghao Zhang, Jie Huang, Mingde Yao, Zizheng Yang, Hu Yu, Man Zhou, and Feng Zhao. Ingredient-oriented multi-degradation learning for image restoration. In *CVPR*, 2023.

[34] Vaishnav Potlapalli, Syed Waqas Zamir, Salman H Khan, and Fahad Shahbaz Khan. Promptir: Prompting for all-in-one image restoration. In *NeurIPS*, 2023.

[35] Eduard Zamfir, Zongwei Wu, Nancy Mehta, Yuedong Tan, Danda Pani Paudel, Yulun Zhang, and Radu Timofte. Complexity experts are task-discriminative learners for any image restoration. In *CVPR*, 2025.

[36] Marcos V Conde, Gregor Geigle, and Radu Timofte. High-quality image restoration following human instructions. In *ECCV*, 2024.

[37] Yuning Cui, Syed Waqas Zamir, Salman Khan, Alois Knoll, Mubarak Shah, and Fahad Shahbaz Khan. AdaIR: Adaptive all-in-one image restoration via frequency mining and modulation. In *ICLR*, 2025.

[38] Yuang Ai, Huaibo Huang, Xiaoqiang Zhou, Jiexiang Wang, and Ran He. Multimodal prompt perceiver: Empower adaptiveness generalizability and fidelity for all-in-one image restoration. In *CVPR*, 2024.

[39] Fanghua Yu, Jinjin Gu, Zheyuan Li, Jinfan Hu, Xiangtao Kong, Xintao Wang, Jingwen He, Yu Qiao, and Chao Dong. Scaling up to excellence: Practicing model scaling for photo-realistic image restoration in the wild. In *CVPR*, 2024.

[40] Yuandong Pu, Le Zhuo, Kaiwen Zhu, Liangbin Xie, Wenlong Zhang, Xiangyu Chen, Pneg Gao, Yu Qiao, Chao Dong, and Yihao Liu. Lumina-omnilv: A unified multimodal framework for general low-level vision. *arXiv preprint arXiv:2504.04903*, 2025.

[41] Ziwei Luo, Fredrik K Gustafsson, Zheng Zhao, Jens Sjölund, and Thomas B Schön. Controlling vision-language models for universal image restoration. In *ICLR*, 2024.

[42] Yu Guo, Yuan Gao, Yuxu Lu, Huilin Zhu, Ryan Wen Liu, and Shengfeng He. Onerestore: A universal restoration framework for composite degradation. In *ECCV*, 2024.

[43] Shangchen Zhou, Chongyi Li, and Chen Change Loy. Lednet: Joint low-light enhancement and deblurring in the dark. In *ECCV*, 2022.

[44] Daniel Feijoo, Juan C Benito, Alvaro Garcia, and Marcos V Conde. Darkir: Robust low-light image restoration. In *CVPR*, 2025.

[45] Wenbin Zou, Hongxia Gao, Tian Ye, Liang Chen, Weipeng Yang, Shasha Huang, Hongsheng Chen, and Sixiang Chen. Vqcnir: Clearer night image restoration with vector-quantized codebook. In *AAAI*, 2024.

[46] Xin Su, Chen Wu, Yu Zhang, Chen Lyu, and Zhuoran Zheng. Adaqual-diff: Diffusion-based image restoration via adaptive quality prompting. *arXiv preprint arXiv:2504.12605*, 2025.

[47] Yawei Li, Yuchen Fan, Xiaoyu Xiang, Denis Demandolx, Rakesh Ranjan, Radu Timofte, and Luc Van Gool. Efficient and explicit modelling of image hierarchies for image restoration. In *CVPR*, 2023.

[48] Yuning Cui, Wenqi Ren, Sining Yang, Xiaochun Cao, and Alois Knoll. Irnext: Rethinking convolutional network design for image restoration. In *ICML*, 2023.

[49] Man Zhou, Jie Huang, Chun-Le Guo, and Chongyi Li. Fourmer: An efficient global modeling paradigm for image restoration. In *ICML*, 2023.

[50] Hu Yu, Naishan Zheng, Man Zhou, Jie Huang, Zeyu Xiao, and Feng Zhao. Frequency and spatial dual guidance for image dehazing. In *ECCV*, 2022.

[51] Chongyi Li, Chun-Le Guo, man zhou, Zhexin Liang, Shangchen Zhou, Ruicheng Feng, and Chen Change Loy. Embedding fourier for ultra-high-definition low-light image enhancement. In *ICLR*, 2023.

[52] Xintian Mao, Yiming Liu, Fengze Liu, Qingli Li, Wei Shen, and Yan Wang. Intriguing findings of frequency selection for image deblurring. In *AAAI*, 2023.

[53] Yichen Zhou, Pan Zhou, and Teck Khim Ng. Efficient cascaded multiscale adaptive network for image restoration. In *ECCV*, 2024.

[54] Hang Guo, Jinmin Li, Tao Dai, Zhihao Ouyang, Xudong Ren, and Shu-Tao Xia. Mambair: A simple baseline for image restoration with state-space model. In *ECCV*, 2024.

[55] Hang Guo, Yong Guo, Yaohua Zha, Yulun Zhang, Wenbo Li, Tao Dai, Shu-Tao Xia, and Yawei Li. Mambairv2: Attentive state space restoration. *arXiv preprint arXiv:2411.15269*, 2024.

[56] Zhen Zou, Hu Yu, Jie Huang, and Feng Zhao. Freqmamba: Viewing mamba from a frequency perspective for image deraining. In *ACM MM*, 2024.

[57] Dong Li, Yidi Liu, Xueyang Fu, Senyan Xu, and Zheng-Jun Zha. Fouriermamba: Fourier learning integration with state space models for image deraining. *arXiv preprint arXiv:2405.19450*, 2024.

[58] Wenbin Zou, Hongxia Gao, Weipeng Yang, and Tongtong Liu. Wave-mamba: Wavelet state space model for ultra-high-definition low-light image enhancement. In *ACM MM*, 2024.

[59] Boyun Li, Haiyu Zhao, Wenxin Wang, Peng Hu, Yuanbiao Gou, and Xi Peng. Mair: A locality-and continuity-preserving mamba for image restoration. In *CVPR*, 2025.

[60] Jiangwei Weng, Zhiqiang Yan, Ying Tai, Jianjun Qian, Jian Yang, and Jun Li. MambaLLIE: Implicit retinex-aware low light enhancement with global-then-local state space. In *NeurIPS*, 2024.

[61] Yuhong He, Long Peng, Qiaosi Yi, Chen Wu, and Lu Wang. Multi-scale representation learning for image restoration with state-space model. *arXiv preprint arXiv:2408.10145*, 2024.

[62] Yuan Shi, Bin Xia, Xiaoyu Jin, Xing Wang, Tianyu Zhao, Xin Xia, Xuefeng Xiao, and Wenming Yang. Vmambair: Visual state space model for image restoration. *IEEE TCSVT*, 2025.

[63] Shangquan Sun, Wenqi Ren, Juxiang Zhou, Jianhou Gan, Rui Wang, and Xiaochun Cao. A hybrid transformer-mamba network for single image deraining. *arXiv preprint arXiv:2409.00410*, 2024.

[64] Juan Wen, Weiyan Hou, Luc Van Gool, and Radu Timofte. Matir: A hybrid mamba-transformer image restoration model. *arXiv preprint arXiv:2501.18401*, 2025.

[65] Long Peng, Xin Di, Zhanfeng Feng, Wenbo Li, Renjing Pei, Yang Wang, Xueyang Fu, Yang Cao, and Zheng-Jun Zha. Directing mamba to complex textures: An efficient texture-aware state space model for image restoration. *arXiv preprint arXiv:2501.16583*, 2025.

[66] Christine A Curcio, Kenneth R Sloan, Robert E Kalina, and Anita E Hendrickson. Human photoreceptor topography. *Journal of comparative neurology*, 1990.

[67] Matteo Toscani, Karl R Gegenfurtner, and Matteo Valsecchi. Foveal to peripheral extrapolation of brightness within objects. *Journal of vision*, 2017.

[68] Emma EM Stewart, Matteo Valsecchi, and Alexander C Schütz. A review of interactions between peripheral and foveal vision. *Journal of vision*, 2020.

[69] Kwang In Kim and Younghee Kwon. Single-image super-resolution using sparse regression and natural image prior. *IEEE TPAMI*, 2010.

[70] Kaiming He, Jian Sun, and Xiaoou Tang. Single image haze removal using dark channel prior. *IEEE TPAMI*, 2010.

[71] Kaihao Zhang, Wenqi Ren, Wenhan Luo, Wei-Sheng Lai, Björn Stenger, Ming-Hsuan Yang, and Hongdong Li. Deep image deblurring: A survey. *IJCV*, 2022.

[72] Hang Dong, Jinshan Pan, Lei Xiang, Zhe Hu, Xinyi Zhang, Fei Wang, and Ming-Hsuan Yang. Multi-scale boosted dehazing network with dense feature fusion. In *CVPR*, 2020.

[73] Yuning Cui, Yi Tao, Wenqi Ren, and Alois Knoll. Dual-domain attention for image deblurring. In *AAAI*, 2023.

[74] Wei-Ting Chen, Hao-Yu Fang, Cheng-Lin Hsieh, Cheng-Che Tsai, I Chen, Jian-Jiun Ding, Sy-Yen Kuo, et al. All snow removed: Single image desnowing algorithm using hierarchical dual-tree complex wavelet representation and contradict channel loss. In *ICCV*, 2021.

[75] Yuning Cui, Qiang Wang, Chaopeng Li, Wenqi Ren, and Alois Knoll. Eenet: An effective and efficient network for single image dehazing. *PR*, 2025.

[76] Xiongfei Su, Siyuan Li, Yuning Cui, Miao Cao, Yulun Zhang, Zheng Chen, Zongliang Wu, Zedong Wang, Yuanlong Zhang, and Xin Yuan. Prior-guided hierarchical harmonization network for efficient image dehazing. In *AAAI*, 2025.

[77] Sixiang Chen, Tian Ye, Yun Liu, Taodong Liao, Jingxia Jiang, Erkang Chen, and Peng Chen. Msp-former: Multi-scale projection transformer for single image desnowing. In *ICASSP*, 2023.

[78] Jiangang Wang, Yuning Cui, Yawen Li, Wenqi Ren, and Xiaochun Cao. Omnidirectional image super-resolution via bi-projection fusion. In *AAAI*, 2024.

[79] Yuning Cui, Wenqi Ren, Xiaochun Cao, and Alois Knoll. Image restoration via frequency selection. *IEEE TPAMI*, 2023.

[80] Yuning Cui, Jianyong Zhu, and Alois Knoll. Enhancing perception for autonomous vehicles: A multi-scale feature modulation network for image restoration. *IEEE TITS*, 2025.

[81] Yuning Cui, Mingyu Liu, Wenqi Ren, and Alois Knoll. Modumer: Modulating transformer for image restoration. *IEEE TNNLS*, 2025.

[82] Yuning Cui, Yi Tao, Zhenshan Bing, Wenqi Ren, Xinwei Gao, Xiaochun Cao, Kai Huang, and Alois Knoll. Selective frequency network for image restoration. In *ICLR*, 2023.

[83] Yuning Cui and Alois Knoll. Enhancing local–global representation learning for image restoration. *IEEE TII*, 2024.

[84] Shangquan Sun, Wenqi Ren, Xinwei Gao, Rui Wang, and Xiaochun Cao. Restoring images in adverse weather conditions via histogram transformer. In *ECCV*, 2024.

[85] Yuning Cui, Wenqi Ren, and Alois Knoll. Exploring the potential of pooling techniques for universal image restoration. *IEEE TIP*, 2025.

[86] Jingbo Lin, Zhilu Zhang, Yuxiang Wei, Dongwei Ren, Dongsheng Jiang, Qi Tian, and Wangmeng Zuo. Improving image restoration through removing degradations in textual representations. In *CVPR*, 2024.

[87] Yuning Cui, Wenqi Ren, and Alois Knoll. Omni-kernel modulation for universal image restoration. *IEEE TCSVT*, 2024.

[88] Mingyu Liu, Yuning Cui, Xin Liu, Leah Strand, Huilin Yin, and Alois Knoll. Drfir: A dimensionality reduction framework for all-in-one image restoration in spatial and frequency domains. *ESWA*, 2025.

[89] Hao Li, Xiang Chen, Jiangxin Dong, Jinhui Tang, and Jinshan Pan. Foundir: Unleashing million-scale training data to advance foundation models for image restoration. *arXiv preprint arXiv:2412.01427*, 2024.

[90] Jaesung Rim, Haeyun Lee, Jucheol Won, and Sunghyun Cho. Real-world blur dataset for learning and benchmarking deblurring algorithms. In *ECCV*, 2020.

[91] Mingyu Liu, Yuning Cui, Wenqi Ren, Juxiang Zhou, and Alois C Knoll. Liednet: A lightweight network for low-light enhancement and deblurring. *IEEE TCSVT*, 2025.

[92] Qiang Wang, Yuning Cui, Yawen Li, Yaping Ruan, Ben Zhu, and Wenqi Ren. Rffnet: Towards robust and flexible fusion for low-light image denoising. In *ACM MM*, 2024.

[93] Yuning Cui, Mingyu Liu, Xiongfei Su, and Alois Knoll. Frequency-prompted image restoration to enhance perception in intelligent transportation systems. *IEEE TITS*, 2025.

[94] Jingbo Lin, Zhilu Zhang, Wenbo Li, Renjing Pei, Hang Xu, Hongzhi Zhang, and Wangmeng Zuo. Unirestorer: Universal image restoration via adaptively estimating image degradation at proper granularity. *arXiv preprint arXiv:2412.20157*, 2024.

[95] Mingyu Liu, Yuning Cui, Leah Strand, Xingcheng Zhou, Jiajie Zhang, and C Alois Knoll. Mambasflnet: A mamba-based model for low-light image enhancement with spatial and frequency features. In *IROS*, 2025.

[96] Mingyu Liu, Jiong Xu, Yuning Cui, Xiaobin Hu, Leah Strand, Huilin Yin, and Alois C Knoll. Ilvmamba: Illumination-aware lightweight visual mamba framework for efficient high-resolution image enhancement. *IEEE TAI*, 2025.

[97] Kai Liu, Haotong Qin, Yong Guo, Xin Yuan, Linghe Kong, Guihai Chen, and Yulun Zhang. 2dquant: Low-bit post-training quantization for image super-resolution. *NeurIPS*, 2024.

[98] Haotong Qin, Yulun Zhang, Yifu Ding, Xianglong Liu, Martin Danelljan, Fisher Yu, et al. Quantsr: accurate low-bit quantization for efficient image super-resolution. *NeurIPS*, 2023.

[99] Yujie Chen, Haotong Qin, Zhang Zhang, Michelo Magno, Luca Benini, and Yawei Li. Q-mambair: Accurate quantized mamba for efficient image restoration. *arXiv preprint arXiv:2503.21970*, 2025.

[100] Bahri Batuhan Bilecen and Mustafa Ayazoglu. Bicubic++: Slim, slimmer, slimmest-designing an industry-grade super-resolution network. In *CVPR*, 2023.

[101] Yunshuai Zhou, Junbo Qiao, Jincheng Liao, Wei Li, Simiao Li, Jiao Xie, Yunhang Shen, Jie Hu, and Shaohui Lin. Dynamic contrastive knowledge distillation for efficient image restoration. In *AAAI*, 2025.

[102] Wei-Ting Chen, Hao-Yu Fang, Jian-Jiun Ding, Cheng-Che Tsai, and Sy-Yen Kuo. Jstasr: Joint size and transparency-aware snow removal algorithm based on modified partial convolution and veiling effect removal. In *ECCV*, 2020.

[103] Boyi Li, Wenqi Ren, Dengpan Fu, Dacheng Tao, Dan Feng, Wenjun Zeng, and Zhangyang Wang. Benchmarking single-image dehazing and beyond. *IEEE TIP*, 2018.

[104] Ye Liu, Lei Zhu, Shunda Pei, Huazhu Fu, Jing Qin, Qing Zhang, Liang Wan, and Wei Feng. From synthetic to real: Image dehazing collaborating with unlabeled real data. In *ACM MM*, 2021.

[105] Wenhan Yang, Wenjing Wang, Haofeng Huang, Shiqi Wang, and Jiaying Liu. Sparse gradient regularized deep retinex network for robust low-light image enhancement. *IEEE TIP*, 2021.

[106] Rui Qian, Robby T Tan, Wenhan Yang, Jiajun Su, and Jiaying Liu. Attentive generative adversarial network for raindrop removal from a single image. In *CVPR*, 2018.

[107] Shihao Zhou, Duosheng Chen, Jinshan Pan, Jinglei Shi, and Jufeng Yang. Adapt or perish: Adaptive sparse transformer with attentive feature refinement for image restoration. In *CVPR*, 2024.

[108] He Zhang and Vishal M Patel. Density-aware single image de-raining using a multi-stream dense network. In *CVPR*, 2018.

[109] Tianyu Wang, Xin Yang, Ke Xu, Shaozhe Chen, Qiang Zhang, and Rynson W.H. Lau. Spatial attentive single-image deraining with a high quality real rain dataset. In *CVPR*, 2019.

[110] Xiang Chen, Jinshan Pan, and Jiangxin Dong. Bidirectional multi-scale implicit neural representations for image deraining. In *CVPR*, 2024.

[111] Zixuan Chen, Zewei He, and Zhe-Ming Lu. Dea-net: Single image dehazing based on detail-enhanced convolution and content-guided attention. *IEEE TIP*, 2024.

[112] Tian Ye, Yunchen Zhang, Mingchao Jiang, Liang Chen, Yun Liu, Sixiang Chen, and Erkang Chen. Perceiving and modeling density for image dehazing. In *ECCV*, 2022.

[113] Syed Waqas Zamir, Aditya Arora, Salman Khan, Munawar Hayat, Fahad Shahbaz Khan, Ming-Hsuan Yang, and Ling Shao. Learning enriched features for real image restoration and enhancement. In *ECCV*, 2020.

[114] Xiaogang Xu, Ruixing Wang, Chi-Wing Fu, and Jiaya Jia. Snr-aware low-light image enhancement. In *CVPR*, 2022.

[115] Jie Xiao, Xueyang Fu, Aiping Liu, Feng Wu, and Zheng-Jun Zha. Image de-raining transformer. *IEEE TPAMI*, 2022.

[116] Zhengzhong Tu, Hossein Talebi, Han Zhang, Feng Yang, Peyman Milanfar, Alan Bovik, and Yinxiao Li. Maxim: Multi-axis mlp for image processing. In *CVPR*, 2022.

[117] Tian Ye, Sixiang Chen, Jinbin Bai, Jun Shi, Chenghao Xue, Jingxia Jiang, Junjie Yin, Erkang Chen, and Yun Liu. Adverse weather removal with codebook priors. In *ICCV*, 2023.

[118] Shihao Zhou, Jinshan Pan, Jinglei Shi, Duosheng Chen, Lishen Qu, and Jufeng Yang. Seeing the unseen: A frequency prompt guided transformer for image restoration. In *ECCV*, 2024.

[119] Gang Wu, Junjun Jiang, Kui Jiang, and Xianming Liu. Harmony in diversity: Improving all-in-one image restoration via multi-task collaboration. In *ACM MM*, 2024.

[120] Huiyu Duan, Xiongkuo Min, Sijing Wu, Wei Shen, and Guangtao Zhai. Uniprocessor: a text-induced unified low-level image processor. In *ECCV*, 2024.

[121] Wenhan Yang, Robby T. Tan, Jiashi Feng, Jiaying Liu, Zongming Guo, and Shuicheng Yan. Deep joint rain detection and removal from a single image. In *CVPR*, 2017.

[122] Tao Wang, Kaihao Zhang, Ziqian Shao, Wenhan Luo, Bjorn Stenger, Tong Lu, Tae-Kyun Kim, Wei Liu, and Hongdong Li. Gridformer: Residual dense transformer with grid structure for image restoration in adverse weather conditions. *IJCV*, 2024.

[123] David Martin, Charless Fowlkes, Doron Tal, and Jitendra Malik. A database of human segmented natural images and its application to evaluating segmentation algorithms and measuring ecological statistics. In *ICCV*, 2001.

[124] Seungjun Nah, Tae Hyun Kim, and Kyoung Mu Lee. Deep multi-scale convolutional neural network for dynamic scene deblurring. In *CVPR*, 2017.

[125] Chen Wei, Wenjing Wang, Wenhan Yang, and Jiaying Liu. Deep retinex decomposition for low-light enhancement. In *BMVC*, 2018.

[126] Lingshun Kong, Jiangxin Dong, Jianjun Ge, Mingqiang Li, and Jinshan Pan. Efficient frequency domain-based transformers for high-quality image deblurring. In *CVPR*, 2023.

[127] Jia-Bin Huang, Abhishek Singh, and Narendra Ahuja. Single image super-resolution from transformed self-exemplars. In *CVPR*, 2015.

[128] Rich Franzen. Kodak lossless true color image suite. `http://r0k.us/graphics/kodak/`, 1999. Online accessed 24 Oct 2021.

[129] Jeya Maria Jose Valanarasu, Rajeev Yasarla, and Vishal M. Patel. Transweather: Transformer-based restoration of images degraded by adverse weather conditions. In *CVPR*, 2022.

[130] Pablo Arbelaez, Michael Maire, Charless Fowlkes, and Jitendra Malik. Contour detection and hierarchical image segmentation. *IEEE TPAMI*, 2010.

[131] Kede Ma, Zhengfang Duanmu, Qingbo Wu, Zhou Wang, Hongwei Yong, Hongliang Li, and Lei Zhang. Waterloo exploration database: New challenges for image quality assessment models. *IEEE TIP*, 2016.

[132] Zhou Wang, Alan C Bovik, Hamid R Sheikh, and Eero P Simoncelli. Image quality assessment: from error visibility to structural similarity. *IEEE TIP*, 2004.

[133] Richard Zhang, Phillip Isola, Alexei A Efros, Eli Shechtman, and Oliver Wang. The unreasonable effectiveness of deep features as a perceptual metric. In *CVPR*, 2018.

[134] Yasheng Sun, Bohan Li, Mingchen Zhuge, Deng-Ping Fan, Salman Khan, Fahad Shahbaz Khan, and Hideki Koike. Connecting dreams with visual brainstorming instruction. *Visual Intelligence*, 2025.

NeurIPS Paper Checklist

1. **Claims**

   Question: Do the main claims made in the abstract and introduction accurately reflect the paper's contributions and scope?

   Answer: [Yes]

   Justification: This paper introduces a bio-inspired efficient image restoration network that achieves state-of-the-art performance on a range of tasks. We reported the numerical results in the tables and illustrated the visual results in the figures.

   Guidelines:

   - The answer NA means that the abstract and introduction do not include the claims made in the paper.
   - The abstract and/or introduction should clearly state the claims made, including the contributions made in the paper and important assumptions and limitations. A No or NA answer to this question will not be perceived well by the reviewers.
   - The claims made should match theoretical and experimental results, and reflect how much the results can be expected to generalize to other settings.
   - It is fine to include aspirational goals as motivation as long as it is clear that these goals are not attained by the paper.

2. **Limitations**

   Question: Does the paper discuss the limitations of the work performed by the authors?

   Answer: [Yes]

   Justification: Please see the Section A.5

   Guidelines:

   - The answer NA means that the paper has no limitation while the answer No means that the paper has limitations, but those are not discussed in the paper.
   - The authors are encouraged to create a separate "Limitations" section in their paper.

- The paper should point out any strong assumptions and how robust the results are to violations of these assumptions (e.g., independence assumptions, noiseless settings, model well-specification, asymptotic approximations only holding locally). The authors should reflect on how these assumptions might be violated in practice and what the implications would be.
- The authors should reflect on the scope of the claims made, e.g., if the approach was only tested on a few datasets or with a few runs. In general, empirical results often depend on implicit assumptions, which should be articulated.
- The authors should reflect on the factors that influence the performance of the approach. For example, a facial recognition algorithm may perform poorly when image resolution is low or images are taken in low lighting. Or a speech-to-text system might not be used reliably to provide closed captions for online lectures because it fails to handle technical jargon.
- The authors should discuss the computational efficiency of the proposed algorithms and how they scale with dataset size.
- If applicable, the authors should discuss possible limitations of their approach to address problems of privacy and fairness.
- While the authors might fear that complete honesty about limitations might be used by reviewers as grounds for rejection, a worse outcome might be that reviewers discover limitations that aren't acknowledged in the paper. The authors should use their best judgment and recognize that individual actions in favor of transparency play an important role in developing norms that preserve the integrity of the community. Reviewers will be specifically instructed to not penalize honesty concerning limitations.

3. **Theory assumptions and proofs**

   Question: For each theoretical result, does the paper provide the full set of assumptions and a complete (and correct) proof?

   Answer: [NA]

   Justification: The paper does not include theoretical results.

   Guidelines:

   - The answer NA means that the paper does not include theoretical results.
   - All the theorems, formulas, and proofs in the paper should be numbered and cross-referenced.
   - All assumptions should be clearly stated or referenced in the statement of any theorems.
   - The proofs can either appear in the main paper or the supplemental material, but if they appear in the supplemental material, the authors are encouraged to provide a short proof sketch to provide intuition.
   - Inversely, any informal proof provided in the core of the paper should be complemented by formal proofs provided in appendix or supplemental material.
   - Theorems and Lemmas that the proof relies upon should be properly referenced.

4. **Experimental result reproducibility**

   Question: Does the paper fully disclose all the information needed to reproduce the main experimental results of the paper to the extent that it affects the main claims and/or conclusions of the paper (regardless of whether the code and data are provided or not)?

   Answer: [Yes]

   Justification: We provided the implementation details in Section A.5, and we do not use any training tricks to improve performance. Our code and pre-trained models will be released.

   Guidelines:

   - The answer NA means that the paper does not include experiments.
   - If the paper includes experiments, a No answer to this question will not be perceived well by the reviewers: Making the paper reproducible is important, regardless of whether the code and data are provided or not.
   - If the contribution is a dataset and/or model, the authors should describe the steps taken to make their results reproducible or verifiable.

- Depending on the contribution, reproducibility can be accomplished in various ways. For example, if the contribution is a novel architecture, describing the architecture fully might suffice, or if the contribution is a specific model and empirical evaluation, it may be necessary to either make it possible for others to replicate the model with the same dataset, or provide access to the model. In general. releasing code and data is often one good way to accomplish this, but reproducibility can also be provided via detailed instructions for how to replicate the results, access to a hosted model (e.g., in the case of a large language model), releasing of a model checkpoint, or other means that are appropriate to the research performed.
- While NeurIPS does not require releasing code, the conference does require all submissions to provide some reasonable avenue for reproducibility, which may depend on the nature of the contribution. For example
  (a) If the contribution is primarily a new algorithm, the paper should make it clear how to reproduce that algorithm.
  (b) If the contribution is primarily a new model architecture, the paper should describe the architecture clearly and fully.
  (c) If the contribution is a new model (e.g., a large language model), then there should either be a way to access this model for reproducing the results or a way to reproduce the model (e.g., with an open-source dataset or instructions for how to construct the dataset).
  (d) We recognize that reproducibility may be tricky in some cases, in which case authors are welcome to describe the particular way they provide for reproducibility. In the case of closed-source models, it may be that access to the model is limited in some way (e.g., to registered users), but it should be possible for other researchers to have some path to reproducing or verifying the results.

5. **Open access to data and code**

   Question: Does the paper provide open access to the data and code, with sufficient instructions to faithfully reproduce the main experimental results, as described in supplemental material?

   Answer: [Yes]

   Justification: We have correctly cited the data we used, and we will make our code and models available publicly.

   Guidelines:

   - The answer NA means that paper does not include experiments requiring code.
   - Please see the NeurIPS code and data submission guidelines (`https://nips.cc/public/guides/CodeSubmissionPolicy`) for more details.
   - While we encourage the release of code and data, we understand that this might not be possible, so "No" is an acceptable answer. Papers cannot be rejected simply for not including code, unless this is central to the contribution (e.g., for a new open-source benchmark).
   - The instructions should contain the exact command and environment needed to run to reproduce the results. See the NeurIPS code and data submission guidelines (`https://nips.cc/public/guides/CodeSubmissionPolicy`) for more details.
   - The authors should provide instructions on data access and preparation, including how to access the raw data, preprocessed data, intermediate data, and generated data, etc.
   - The authors should provide scripts to reproduce all experimental results for the new proposed method and baselines. If only a subset of experiments are reproducible, they should state which ones are omitted from the script and why.
   - At submission time, to preserve anonymity, the authors should release anonymized versions (if applicable).
   - Providing as much information as possible in supplemental material (appended to the paper) is recommended, but including URLs to data and code is permitted.

6. **Experimental setting/details**

   Question: Does the paper specify all the training and test details (e.g., data splits, hyperparameters, how they were chosen, type of optimizer, etc.) necessary to understand the results?

Answer: [Yes]

Justification: Please refer to Section A.1.

Guidelines:

- The answer NA means that the paper does not include experiments.
- The experimental setting should be presented in the core of the paper to a level of detail that is necessary to appreciate the results and make sense of them.
- The full details can be provided either with the code, in appendix, or as supplemental material.

7. **Experiment statistical significance**

Question: Does the paper report error bars suitably and correctly defined or other appropriate information about the statistical significance of the experiments?

Answer: [No]

Justification: The paper does not report error bars following previous image restoration methods.

Guidelines:

- The answer NA means that the paper does not include experiments.
- The authors should answer "Yes" if the results are accompanied by error bars, confidence intervals, or statistical significance tests, at least for the experiments that support the main claims of the paper.
- The factors of variability that the error bars are capturing should be clearly stated (for example, train/test split, initialization, random drawing of some parameter, or overall run with given experimental conditions).
- The method for calculating the error bars should be explained (closed form formula, call to a library function, bootstrap, etc.)
- The assumptions made should be given (e.g., Normally distributed errors).
- It should be clear whether the error bar is the standard deviation or the standard error of the mean.
- It is OK to report 1-sigma error bars, but one should state it. The authors should preferably report a 2-sigma error bar than state that they have a 96% CI, if the hypothesis of Normality of errors is not verified.
- For asymmetric distributions, the authors should be careful not to show in tables or figures symmetric error bars that would yield results that are out of range (e.g. negative error rates).
- If error bars are reported in tables or plots, The authors should explain in the text how they were calculated and reference the corresponding figures or tables in the text.

8. **Experiments compute resources**

Question: For each experiment, does the paper provide sufficient information on the computer resources (type of compute workers, memory, time of execution) needed to reproduce the experiments?

Answer: [Yes]

Justification: Please see Section A.1

Guidelines:

- The answer NA means that the paper does not include experiments.
- The paper should indicate the type of compute workers CPU or GPU, internal cluster, or cloud provider, including relevant memory and storage.
- The paper should provide the amount of compute required for each of the individual experimental runs as well as estimate the total compute.
- The paper should disclose whether the full research project required more compute than the experiments reported in the paper (e.g., preliminary or failed experiments that didn't make it into the paper).

9. **Code of ethics**

Question: Does the research conducted in the paper conform, in every respect, with the NeurIPS Code of Ethics `https://neurips.cc/public/EthicsGuidelines`?

Answer: [Yes]

Justification: Our research conforms with the NeurIPS Code of Ethics.

Guidelines:

- The answer NA means that the authors have not reviewed the NeurIPS Code of Ethics.
- If the authors answer No, they should explain the special circumstances that require a deviation from the Code of Ethics.
- The authors should make sure to preserve anonymity (e.g., if there is a special consideration due to laws or regulations in their jurisdiction).

10. **Broader impacts**

Question: Does the paper discuss both potential positive societal impacts and negative societal impacts of the work performed?

Answer: [Yes]

Justification: Please refer to Section A.5

Guidelines:

- The answer NA means that there is no societal impact of the work performed.
- If the authors answer NA or No, they should explain why their work has no societal impact or why the paper does not address societal impact.
- Examples of negative societal impacts include potential malicious or unintended uses (e.g., disinformation, generating fake profiles, surveillance), fairness considerations (e.g., deployment of technologies that could make decisions that unfairly impact specific groups), privacy considerations, and security considerations.
- The conference expects that many papers will be foundational research and not tied to particular applications, let alone deployments. However, if there is a direct path to any negative applications, the authors should point it out. For example, it is legitimate to point out that an improvement in the quality of generative models could be used to generate deepfakes for disinformation. On the other hand, it is not needed to point out that a generic algorithm for optimizing neural networks could enable people to train models that generate Deepfakes faster.
- The authors should consider possible harms that could arise when the technology is being used as intended and functioning correctly, harms that could arise when the technology is being used as intended but gives incorrect results, and harms following from (intentional or unintentional) misuse of the technology.
- If there are negative societal impacts, the authors could also discuss possible mitigation strategies (e.g., gated release of models, providing defenses in addition to attacks, mechanisms for monitoring misuse, mechanisms to monitor how a system learns from feedback over time, improving the efficiency and accessibility of ML).

11. **Safeguards**

Question: Does the paper describe safeguards that have been put in place for responsible release of data or models that have a high risk for misuse (e.g., pretrained language models, image generators, or scraped datasets)?

Answer: [Yes]

Justification: Please refer to Section A.5

Guidelines:

- The answer NA means that the paper poses no such risks.
- Released models that have a high risk for misuse or dual-use should be released with necessary safeguards to allow for controlled use of the model, for example by requiring that users adhere to usage guidelines or restrictions to access the model or implementing safety filters.
- Datasets that have been scraped from the Internet could pose safety risks. The authors should describe how they avoided releasing unsafe images.

- We recognize that providing effective safeguards is challenging, and many papers do not require this, but we encourage authors to take this into account and make a best faith effort.

12. **Licenses for existing assets**

    Question: Are the creators or original owners of assets (e.g., code, data, models), used in the paper, properly credited and are the license and terms of use explicitly mentioned and properly respected?

    Answer: [Yes]

    Justification: We have cited the datasets used.

    Guidelines:

    - The answer NA means that the paper does not use existing assets.
    - The authors should cite the original paper that produced the code package or dataset.
    - The authors should state which version of the asset is used and, if possible, include a URL.
    - The name of the license (e.g., CC-BY 4.0) should be included for each asset.
    - For scraped data from a particular source (e.g., website), the copyright and terms of service of that source should be provided.
    - If assets are released, the license, copyright information, and terms of use in the package should be provided. For popular datasets, `paperswithcode.com/datasets` has curated licenses for some datasets. Their licensing guide can help determine the license of a dataset.
    - For existing datasets that are re-packaged, both the original license and the license of the derived asset (if it has changed) should be provided.
    - If this information is not available online, the authors are encouraged to reach out to the asset's creators.

13. **New assets**

    Question: Are new assets introduced in the paper well documented and is the documentation provided alongside the assets?

    Answer: [Yes]

    Justification: This paper introduces a new architecture for image restoration, and we will make the code and pre-trained models publicly available.

    Guidelines:

    - The answer NA means that the paper does not release new assets.
    - Researchers should communicate the details of the dataset/code/model as part of their submissions via structured templates. This includes details about training, license, limitations, etc.
    - The paper should discuss whether and how consent was obtained from people whose asset is used.
    - At submission time, remember to anonymize your assets (if applicable). You can either create an anonymized URL or include an anonymized zip file.

14. **Crowdsourcing and research with human subjects**

    Question: For crowdsourcing experiments and research with human subjects, does the paper include the full text of instructions given to participants and screenshots, if applicable, as well as details about compensation (if any)?

    Answer: [NA]

    Justification: The paper does not involve crowdsourcing nor research with human subjects.

    Guidelines:

    - The answer NA means that the paper does not involve crowdsourcing nor research with human subjects.
    - Including this information in the supplemental material is fine, but if the main contribution of the paper involves human subjects, then as much detail as possible should be included in the main paper.

- According to the NeurIPS Code of Ethics, workers involved in data collection, curation, or other labor should be paid at least the minimum wage in the country of the data collector.

15. **Institutional review board (IRB) approvals or equivalent for research with human subjects**

    Question: Does the paper describe potential risks incurred by study participants, whether such risks were disclosed to the subjects, and whether Institutional Review Board (IRB) approvals (or an equivalent approval/review based on the requirements of your country or institution) were obtained?

    Answer: [NA]

    Justification: The paper does not involve crowdsourcing nor research with human subjects.

    Guidelines:

    - The answer NA means that the paper does not involve crowdsourcing nor research with human subjects.
    - Depending on the country in which research is conducted, IRB approval (or equivalent) may be required for any human subjects research. If you obtained IRB approval, you should clearly state this in the paper.
    - We recognize that the procedures for this may vary significantly between institutions and locations, and we expect authors to adhere to the NeurIPS Code of Ethics and the guidelines for their institution.
    - For initial submissions, do not include any information that would break anonymity (if applicable), such as the institution conducting the review.

16. **Declaration of LLM usage**

    Question: Does the paper describe the usage of LLMs if it is an important, original, or non-standard component of the core methods in this research? Note that if the LLM is used only for writing, editing, or formatting purposes and does not impact the core methodology, scientific rigorousness, or originality of the research, declaration is not required.

    Answer: [NA]

    Justification: The core method development in this research does not involve LLMs as any important, original, or non-standard components.

    Guidelines:

    - The answer NA means that the core method development in this research does not involve LLMs as any important, original, or non-standard components.
    - Please refer to our LLM policy (`https://neurips.cc/Conferences/2025/LLM`) for what should or should not be described.

A Technical Appendices and Supplementary Material

A.1 Implementation Details

This subsection presents the implementation details for the three image restoration settings. To accommodate the varying complexities of different datasets and scenarios, we provide three architectural variants of our model: BioIR-T (Tiny), BioIR-B (Base), and BioIR-L (Large). As summarized in Table 9, these variants are scaled by adjusting the number of channels and the number of BioBlocks at each resolution level, while keeping all other architectural components unchanged across versions.

Single-degradation/composite degradation image restoration. Following previous methods [31, 1, 28], the proposed model is trained using the l_1 loss computed in both the spatial and frequency domains, optimized with the Adam optimizer. The initial learning rate is set to 1×10^{-3} and is progressively reduced to 1×10^{-7} using a cosine annealing schedule. Consistent with prior Transformer-based approaches [25], our models are generally trained for 300K iterations. For deraining tasks, evaluation is performed on the Y channel in the YCbCr color space, following standard protocols [107, 21, 110]. All experiments are conducted using PyTorch on NVIDIA Tesla A100 80G GPUs.

Table 9: The configurations of different BioIR variants.

BioIR	Channels	BioBlocks	Parameters	FLOPs
Tiny (T)	[32, 64, 128, 128, 64, 32, 32]	[1, 1, 2, 2, 1, 1, 4]	1.32M	16.65G
Base (B)	[48, 96, 192, 192, 96, 48, 48]	[3, 3, 6, 6, 3, 3, 4]	7.28M	67.81G
Large (L)	[48, 96, 192, 192, 96, 48, 48]	[6, 6, 14, 14, 6, 6, 4]	15.85M	125.64G

All-in-one image restoration. The datasets used in the two all-in-one image restoration settings are summarized in Table 10. The three-task setting includes dehazing, deraining, and denoising, while the five-task setting additionally incorporates motion deblurring and low-light image enhancement for both training and evaluation. Noisy images are synthesized by adding Gaussian noise with $\sigma \in \{15, 25, 50\}$ to clean images. Our dataset configurations closely follow those adopted in previous all-in-one studies [34, 35, 37, 36].

Following [35], the proposed model is trained using dual-domain l_1 loss functions on 128×128 image patches. The batch size is set to 32, and the model is trained for 100 epochs in the three-task setting and 150 epochs in the five-task setting. The initial learning rate is set to 2×10^{-4}. For data augmentation, random horizontal and vertical flips are applied.

Table 10: Datasets used in the experiments for two all-in-one settings.

Task	Dehazing	Deraining	Denoising	Deblurring	Enhancement
Training set	RESIDE$-\beta$ [103]	Rain100L [121]	BSD400 [130], WED [131]	GoPro [124]	LOLv1 [125]
Test set	SOTS-Outdoor [103]	Rain100L [121]	BSD68 [123], Urban100 [127], Kodak24 [128]	GoPro [124]	LOLv1 [125]

A.2 Additional ablation studies

Table 11: Additional ablation studies for F2P. The kernel size of the depthwise convolution in F2P is set to 7×7.

Method	PSNR	FLOPs	Params
F2P (one-stage, G=3 in Fig. 3(e))	35.85	15.33	1.28
F2P (two-stage, G=3)	36.59	15.33	1.28
F2P (two-stage, G=5)	36.96	15.61	1.29
F2P (two-stage, G=7)	37.08	16.02	1.31

More ablations for F2P. We first conduct experiments to validate the effectiveness of the two-stage design in the F2P module. As reported in Table 11, the one-stage variant, obtained by removing the element-wise multiplication, achieves a PSNR of 35.85 dB, while the proposed two-stage design improves performance to 36.59 dB without introducing additional computational overhead. We

further investigate the impact of the kernel size (G in Fig. 3(e)) used in the dynamic convolution. The results show that performance consistently improves as the kernel size increases. Based on this trade-off between computational cost and accuracy, we select $G = 5$ in our final model.

More ablations for P2F. Similarly, we investigate the impact of increasing the kernel size (K in Fig. 3(d)) of the dynamic convolution in the P2F module. The results, summarized in Table 12, show performance trends across different kernel sizes. To maintain a lightweight design, we adopt $K = 3$ in our final model.

Table 12: Additional ablation studies for P2F. S is set to 16 in P2F.

Method	PSNR	FLOPs	Params
P2F (K=3 in Fig. 3(d))	36.64	15.38	1.25
P2F (K=5)	36.8	17.2	1.30

A.3 Evaluation on perceptual metrics

In addition to PSNR and SSIM [132], this subsection reports evaluation results using the perceptual metric LPIPS [133] to further assess the effectiveness of the proposed model. Table 13 compares our model with leading all-in-one algorithms. As shown, our model achieves the best LPIPS scores on most datasets, demonstrating superior perceptual quality compared to competing methods.

Table 13: Comparisons under the five-task (top) and three-task (bottom) all-in-one image restoration settings, evaluated in terms of LPIPS [133] (lower is better).

Method	*Dehazing* SOTS	*Deraining* Rain100L	*Denoising* (BSD68) $\sigma = 15$	$\sigma = 25$	$\sigma = 50$	*Deblurring* GoPro	*Low-Light* LOLv1
AdaIR$_{\text{ICLR25}}$ [37]	0.0129	0.0139	0.0634	0.1114	0.2105	0.1902	0.1206
MoCE-IR$_{\text{CVPR25}}$ [35]	0.0126	0.0137	0.0610	0.1029	0.1945	0.1444	0.1183
BioIR-L$_{\text{Ours}}$	0.0107	0.0107	0.0569	0.1015	0.1934	0.1450	0.1122
AdaIR$_{\text{ICLR25}}$ [37]	0.0116	0.0118	0.0611	0.1079	0.2112	-	-
MoCE-IR$_{\text{CVPR25}}$ [35]	0.0119	0.0106	0.0575	0.1008	0.1906	-	-
BioIR-L$_{\text{Ours}}$	0.0110	0.0108	0.0509	0.0924	0.1859	-	-

A.4 Additional visual results

This subsection presents additional qualitative results for single-degradation, all-in-one, and composite degradation image restoration tasks, organized as follows:

- Single-degradation: Figure 5 (SRRS [102], desnowing), Figure 6 (Haze4k [104], dehazing), Figure 7 (LOLv2-s [105], enhancement)
- Composite degradation: Figure 8 (LOLBlur [43]), Figure 9 (CDD11 [42]), Figure 10 (Real-LOLBlur [43])
- All-in-one: Figures 11, 12 (Rain100L [121], BSD68 [123], five-task setting)

These results further demonstrate the superior capability of our model in addressing various types of degradations across diverse image restoration scenarios.

A.5 Limitation and Broader Impact

This work presents a bio-inspired image restoration network that achieves state-of-the-art performance across three representative restoration settings, while maintaining high computational efficiency. However, the human visual perception process is highly complex and remains an active area of investigation [68, 134]. The bio-inspired mechanisms proposed in this study represent only a preliminary attempt to mimic this process. Additionally, the current recalibration strategy is implemented using simple element-wise multiplication. Designing more advanced recalibration mechanisms may further improve performance and robustness, which we consider a promising direction for future work.

While this study focuses on the academic advancement of universal image restoration, the proposed algorithm holds potential for various practical applications. It may bring positive social impacts, such as enhancing image quality captured under adverse conditions or with low-end devices. However, it also raises potential concerns, including the risk of privacy leakage when enhancing sensitive content. Nonetheless, we believe the benefits significantly outweigh the risks, and users are encouraged to apply additional privacy-preserving techniques to safeguard sensitive information in images.

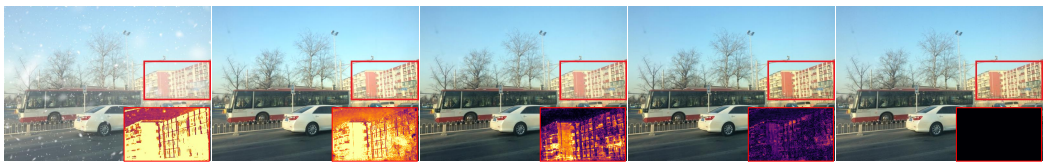

17.17 dB	26.40 dB	29.18 dB	31.83 dB	PSNR/+∞
Snowy Image	ConvIR-B [31]	MBTF V2 [29]	BioIR-B	Reference

Figure 5: Visual results on the SRRS [102] dataset for image desnowing. The bottom-right sub-images present the L_1 error maps computed between the restored and reference regions enclosed by small red boxes, where brighter pixels indicate larger errors, highlighting the superiority of our approach.

11.35 dB	21.81 dB	27.90 dB	30.22 dB	PSNR/+∞
Hazy Image	FSNet [79]	MBTF V2 [29]	BioIR-B	Reference

Figure 6: Visual results on the Haze4k [104] dataset for image dehazing. The bottom-right sub-images present the L_1 error maps computed between the restored and reference regions enclosed by small pink boxes, where brighter pixels indicate larger errors, highlighting the superiority of our approach.

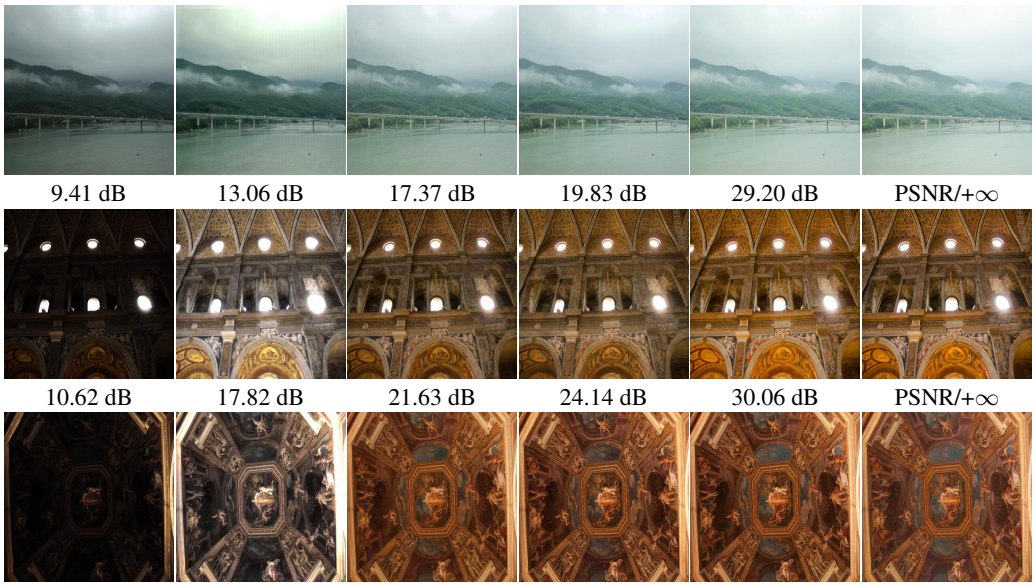

9.41 dB	13.06 dB	17.37 dB	19.83 dB	29.20 dB	PSNR/+∞
10.62 dB	17.82 dB	21.63 dB	24.14 dB	30.06 dB	PSNR/+∞
10.49 dB	16.50 dB	25.13 dB	26.30 dB	27.18 dB	PSNR/+∞
Low-light Image	MIRNet	Retinexformer	MambaLLIE	BioIR-T	Reference

Figure 7: Visual comparison on the LOLv2-s [105] dataset for low-light image enhancement.

7.44 dB	20.66 dB	17.15 dB	26.26 dB	PSNR/+∞
Degraded Image	LEDNet [43]	DarkIR-L [44]	BioIR-T	Reference

Figure 8: Qualitative results on the LOLBlur [43] dataset under composite degradations. Our model achieves more effective brightness restoration and detail recovery from low-light and blurred inputs.

Figure 9: Visual results on the CDD11 [42] dataset for composite degradations.

Figure 10: Generalization evaluation by directly applying the model pretrained on LOLBlur [43] to real-world night blurry images. The top example is from the RealBlur [90] dataset, while the bottom example is captured in an uncontrolled real-world setting. Our model more effectively restores both text details and overall brightness.

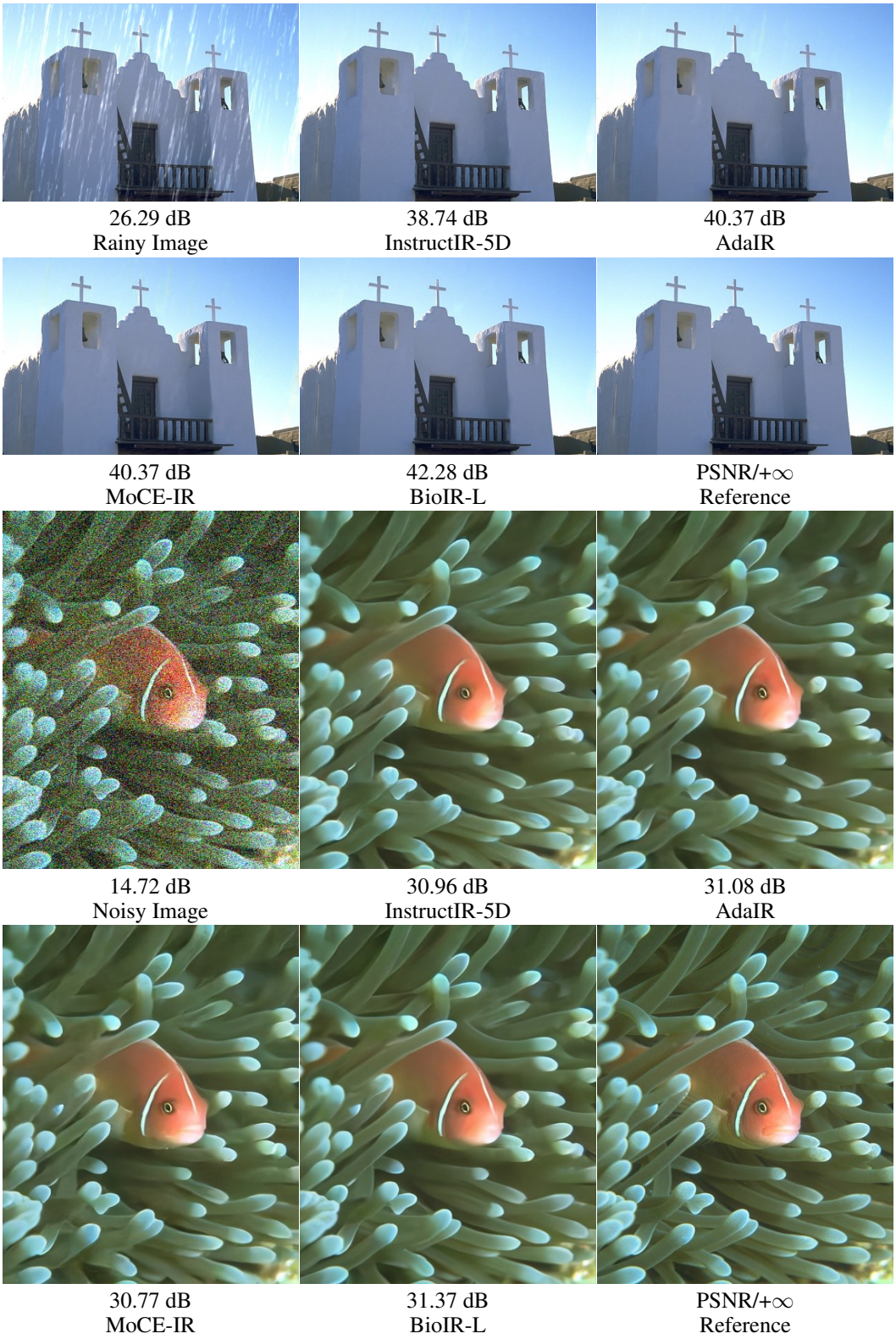

Figure 11: Visual results under the five-task all-in-one setting.

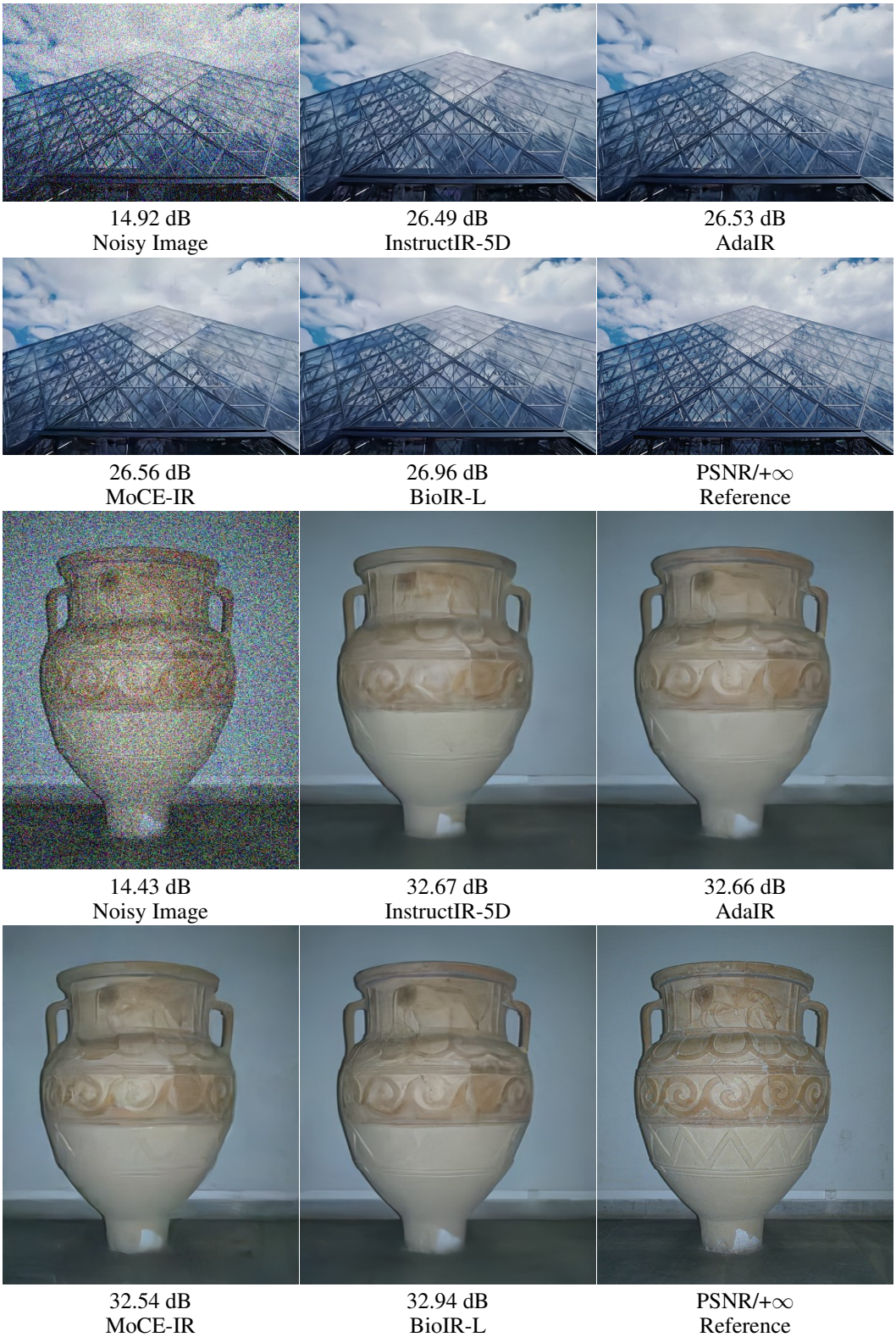

Figure 12: Visual results under the five-task all-in-one setting.